https://doi.org/10.5194/egusphere-2025-2052
Preprint. Discussion started: 19 June 2025

Measurement report: Lidar observations of cirrus cloud properties with CALIPSO from midlatitudes towards high-latitudes

Qiang Li and Silke Groß

Deutsches Zentrum für Luft- und Raumfahrt, Institut für Physik der Atmosphäre, D-82234 Oberpfaffenhofen, Germany,

Correspondence: Qiang Li (qiang.li@dlr.de)

Abstract. Cirrus clouds play a crucial role in the Earth's radiation budget. However, direct observations and model simulations of cirrus at high-latitudes are still sparse. In this study, we present the occurrence rate (OR) and geometrical thickness as well as extinction and particle linear depolarization ratio (PLDR) of cirrus at midlatitudes (35–60°N; 30°W–30°E) and high-latitudes (60–80°N; 30°W–30°E) using lidar measurements of CALIPSO in the years 2014 and 2018–2021. The results indicate a distinct seasonal cycle in the cirrus occurrence and optical properties. The seasonality in ORs and geometrical thicknesses generally becomes more pronounced with increasing latitude, while the altitude ranges of cirrus decrease with increasing latitude. The extinction coefficients decrease with increasing altitude at both high- and midlatitudes and are, in addition, larger at midlatitudes than at high-latitudes in all seasons. The calculated effective optical depths also show larger values at midlatitudes than at high-latitudes, while the differences across latitudes in winter are negligible. The distributions of PLDR in each 5-degree latitude bin show a general decrease with increasing latitude, leading to a remarkable latitudinal difference with larger values at midlatitudes than at high-latitudes. Finally, we compare the aerosol concentrations at different latitudes acting as ice-nucleating particles (INPs) to trigger heterogeneous freezing, as reported in previous studies. It turns out that aerosols such as mineral dust and soot (including aviation-induced soot) indicate much larger concentrations at midlatitudes than at high-latitudes.

1 Introduction

Cirrus clouds are composed entirely of ice crystals with a variety of sizes and shapes and widely occur in the cold upper troposphere (Liou, 1986; Heymsfield et al., 2017; Krämer et al., 2020). Cirrus clouds play a crucial role in modifying the Earth's radiation budget and hydrological cycle (Liou, 1986; Wang et al., 1996; Wylie and Menzel, 1999; Sassen and Benson, 2001; Sassen et al., 2008; Nazaryan et al., 2008). They can efficiently trap outgoing long-wave radiation emitted from the Earth's surface and underlying atmosphere to cause surface warming (greenhouse effect). They also reflect incoming short-wave solar radiation back into space, which results in a cooling effect (albedo effect). The net radiative effect depends on the cloud geometrical, optical, and microphysical properties (e.g. ice crystal size, shape, and orientation in space), which are further determined by the ice formation pathways depending on the surrounding environment (e.g. temperature, humidity, vertical motion, and presence of INPs) (e.g. Fu and Liou, 1993; Zhang et al., 1999; Zerefos et al., 2003; Stephens et al., 2004; Bailey and Hallett, 2004, 2009; Baran, 2009; Campbell et al., 2016; Krämer et al., 2016; Heymsfield et al., 2017; Marsing et

https://doi.org/10.5194/egusphere-2025-2052
Preprint. Discussion started: 19 June 2025

al., 2023). Optically-thin and high cirrus clouds are presumed to have a warming effect because they are nearly transparent to solar incident radiation but still capable to absorb outgoing long-wave radiation (Liou, 1986). Cirrus clouds are typically classified into two types according to the different formation mechanisms and microphysical properties (Krämer et al., 2016; Luebke et al., 2016; Heymsfield et al., 2017). The first type is in situ origin cirrus with ice crystals forming directly from water vapor mainly through homogeneous freezing in cold temperatures (below -38°C) and also through heterogeneous freezing in the presence of INPs. The second type is liquid origin cirrus, which form from glaciation of mixed-phase clouds when they are lifted up into the regions with cold enough temperatures. Satellite observations and climate models reveal that cirrus clouds are one of the most ubiquitous cloud genera with a wide coverage of the Earth's surface, but their fractions display a strong latitude dependence with a maximum of up to 70% over the tropics, approximately 30% over the midlatitudes, and decreasing towards the poles ($\sim$ 10%) (Liou, 1986; Sassen et al., 2008; Nazaryan et al., 2008; Hong and Liu, 2015).

Midlatitude cirrus clouds are of particular importance, not only because they significantly influence the Earth's radiation budget, but also, they interact with the atmospheric dynamics and weather patterns leading to strong uncertainties in their representation in global and regional climate models and numerical weather prediction (NWP) models (Boucher et al., 2013; Kienast-Sjögren et al., 2016; Voigt et al., 2017, 2022; Marquis et al., 2023). They may readily warm or cool the atmosphere during daytime depending on their microphysical properties as well as cloud heights, temperatures, and ice water path (Fu and Liou, 1993; Zhang et al., 1999; Chen et al., 2000; Corti and Peter, 2009). Furthermore, civil aviation takes place mainly in the northern midlatitudes. Aviation emissions lead to the formation of linear contrails and further contrail cirrus which exert a strong influence on the properties of naturally-formed cirrus clouds and contribute a large part of the climate impact of aviation (e.g. Burkhardt and Kärcher, 2011; Tesche et al., 2016; Urbanek et al., 2018; Lee et al., 2021; Li and Groß, 2021, 2022; Groß et al., 2023; *Quaas et al.*, 2024). Since civil aviation over Europe grew strongly before the COVID-19 pandemic and underwent a partial recovery and further increase afterwards in terms of CO2 emission and flight densities, the effects of aviation-induced clouds on our climate are growing significantly. However, there is still a large uncertainty in our understanding of the resulting overall effects (Bock and Burkhardt, 2019; Lee et al., 2021).

In contrast with midlatitudes, cirrus clouds in the Arctic and high-latitude regions are less plentiful and thinner (i.e. lower IWC) (Schiller et al., 2008; Luebke et al., 2013; De La Torre Castro et al., 2023, and references therein). However, they provide a considerable coverage and tend to predominantly warm the atmosphere due to the low elevation of the sun, especially at polar night (Hong and Liu, 2015). It is presumed that there are less efficient INPs available for heterogeneous freezing in the Arctic and high-latitude regions since they are less influenced by anthropogenic pollutants and air traffic than midlatitudes and are lacking in sources of mineral dust and further only small portion of sea salt aerosols can reach cirrus altitudes (Murphy et al., 2019; Wagner et al., 2021). On the other hand, the long-range transport of INPs from midlatitudes (including both natural and anthropogenic sources) to high-latitudes plays an important role in cirrus cloud formation (e.g. *Ratcliffe et al.*, 2024). Especially, smoke aerosols transported across long distances from wildfires in Canada, Alaska, and Siberia frequently impact the Arctic and high-latitude regions by triggering ice crystal formation at lower energy barrier for freezing and by modifying their properties (e.g. Sato et al., 2025). Furthermore, high-latitudes experience more consistent cold temperatures which leads to more stable and drier air masses compared with midlatitudes. In situ origin cirrus clouds are more prevalent

https://doi.org/10.5194/egusphere-2025-2052
Preprint. Discussion started: 19 June 2025

in the high-latitude regions, particularly in polar regions, because of the favorable atmospheric conditions there. Furthermore, deep convection occurs less often at high-latitudes than midlatitudes, which restrains the formation of liquid-origin cirrus clouds. Studies on high-latitude cirrus clouds have been attracting increased attention in recent decades because the near-surface air temperature in the Arctic experiences a faster increase compared to the rest of the world nearly by a factor of four (Rantanen et al., 2022). The enhanced Arctic warming is known as Arctic amplification (AA), which is both a consequence and a driver of feedback processes of climate change (e.g. Serreze et al., 2009). Greenhouse gas emissions due to anthropogenic activities lead to global warming and to reduced sea ice cover in the Arctic. The darker ice-free surface will reduce the albedo and increase absorption of solar radiation in the Arctic, especially during the cold seasons, which contributes to additional warming and strengthens the processes. The effects of AA are not only limited within the Arctic climates, but are presumed to have global implications (Wendisch et al., 2023). With increased evaporation from expanding open water surface due to faster warming by AA, higher humidity levels are induced in the Arctic atmosphere. This process has a potential impact on the precipitation patterns both locally and at midlatitudes since the moisture is transported by the atmospheric circulation (McCrystall et al., 2021). Furthermore, the temperature gradient between high-latitudes and midlatitudes will be weakened due to the faster warming at high-latitudes, which may influence the weather patterns globally and lead to more extreme weather events (e.g. Francis and Vavrus, 2012; Dai and Deng, 2021). A further expected consequence is an increased occurrence of warm air intrusions (WAI) and cold air outbreaks (CAO). Both phenomena play significant roles in shaping weather patterns and atmospheric dynamics as well as the interplay of air masses between the high- and midlatitudes (Woods and Caballero, 2016; Fletcher et al., 2016; Mewes and Jacobi, 2019). WAI can influence cirrus cloud properties by transporting large amounts of moist and warm air masses as well as different ice nucleating particles into the Arctic. CAO extending into midlatitude regions lead to changes in atmospheric conditions (including atmospheric stability, humidity levels and vertical motion) and are associated with many major winter weather disruptions at both high- and midlatitudes. The intrusion of cold and dry air masses from the Arctic can influence the formation and properties of cirrus cloud at midlatitudes (Pithan et al., 2018). Although the understanding of the formation processes and feedback mechanisms regarding AA has been improving thanks to the intensive studies conducted recently with numerous experimental and theoretical efforts, many uncertainties remain (Holland and Bitz, 2003; Serreze et al., 2009; Serreze and Barry, 2011; England et al., 2021; Rantanen et al., 2022; Wendisch et al., 2019, 2023). Especially, the properties of cirrus cloud in the high-latitude regions and their interaction with AA are still not fully understood. Compared to the midlatitudes where multiple measurements are carried out, high-latitudes are rarely probed due to the lack of sounding instruments. Therefore, a detailed study of cirrus cloud properties and their comparison at different latitudes is highly essential to improve our understanding of cirrus clouds on a global scale.

It is well known that light scattered by atmospheric ice particles may exhibit different polarization states from incident light. Computation of the geometric ray tracing technique reveals that changes in polarization states depend on the internal ray paths and, more precisely, increase with increasing hexagonal axis ratio (=length over width) of ice crystals (Takano and Liou, 1989). Particle linear depolarization ratio (PLDR) is a well-defined parameter for evaluating this effect and is widely used to retrieve information on aerosol profiles and ice particle habits, i.e. particle phase, shape, and orientation (Sassen and Zhu, 2009; Freudenthaler et al., 2009; Tesche et al., 2009; Groß et al., 2012, 2013, 2015). In traditional lidar applications, PLDR is

https://doi.org/10.5194/egusphere-2025-2052
Preprint. Discussion started: 19 June 2025

defined as the ratio of power from both polarization components perpendicular and parallel to the transmitted laser source. The extinction coefficient refers to a measure to quantify the attenuation of light due to scattering and absorption by ice crystals within cirrus clouds. In contrast with PLDR, extinction is one of the fundamental characterizing bulk properties of cirrus cloud and depends on the particle number concentration. The vertical distribution of extinction is essential for determining the cloud thickness and an improved knowledge of extinction (and thus optical depth) in cirrus clouds would lead to a better estimation of their general albedo effects. Furthermore, extinction is of crucial importance for radiative transfer calculations in weather prediction and climate models. The parameterization of extinction coefficients in terms of IWC strongly depends on the cloud temperatures and ice particle habits and size distribution (Martin and Platt, 1997). To investigate the latitudinal difference of cirrus cloud properties, we use PLDR, the extinction coefficients (σ_{ci}), and the calculated effective optical depth (τ_{ci}) (i.e. optical thickness) of cirrus clouds calculated as

$$\tau_{\mathrm{ci}} = \int_{r_{\mathrm{b}}}^{r_{\mathrm{t}}} \sigma_{\mathrm{ci}} \, \mathrm{d}z \tag{1}$$

where r_{t} and r_{b} are the cloud-top and cloud-bottom heights of cirrus clouds, respectively.

Many sophisticated ground-based and spaceborne techniques have been developed to observe cirrus clouds. Lidar onboard satellite is the only practical means to probe the atmospheric entities such as clouds on a global scale. Therefore, we use satellite lidar measurements to investigate cirrus cloud properties from midlatitudes towards high-latitudes. In Sect. 2 we will outline the CALIPSO data and methods. Sect. 3 describes our results concerning seasonal variations and long-term trends in cirrus cloud properties and occurrence based on 10-year lidar measurements from March 2010 to February 2020. The dependence of the cirrus cloud properties on the corresponding ambient temperatures as well as the potential impact of aviation are determined and discussed in Sect.4. Our conclusions are finally summarized in Sect.5.

2 Data and methods

The CALIPSO satellite equipped with the CALIOP (Cloud-Aerosol Lidar with Orthogonal Polarization) instrument has been providing a comprehensive dataset of the atmosphere observations since June 2006 and advancing our understanding of the atmospheric aerosols and clouds (Winker et al., 2010; Stephens et al., 2018). After 17 years of successful operation, CALIPSO came to an end in August 2023. As the primary payload of CALIPSO, CALIOP is a dual-wavelength elastic backscatter lidar operating at 532 and 1064 nm and has polarization capability at 532 nm (Winker et al., 2007; Hunt et al., 2009). A feature of CALIOP is to continuously observe altitude-resolved profiles of backscatter intensity from the global atmosphere and to identify the vertical structures of cloud and aerosol layers with a high vertical resolution. This is of substantial advantages for relevant studies. CALIOP is nadir pointing and thus collects data only along the curtain of the CALIPSO track.

In this study, we use the Level 2 5-km cloud profile products containing the coded information of particle extinction, backscatter and particle linear depolarization ratio (PLDR) from all the atmospheric entities and additionally the temperatures in cloud derived from the GEOS-5 data. To distinguish cirrus clouds from other features including aerosols as well as

https://doi.org/10.5194/egusphere-2025-2052
Preprint. Discussion started: 19 June 2025

from non-cirrus clouds, we have applied the vertical feature mask (VFM) developed by the CALIPSO team to yield information on feature types and subtypes by decoding the bit-mapped integers recorded in VFM (e.g. Liu et al., 2004, 2009; Hu et al., 2009; Omar et al., 2009; Vaughan et al., 2009; Winker et al., 2009). In addition, to exclude misclassified mix-phased clouds and noise-contaminated signals, we only consider cloud profiles at temperatures below -38°C (= 235 K). For the description of the CALIOP data in more details, readers are referred to Li and Groß (2021) and references therein. The formation heights of cirrus clouds are closely tied to the local tropopause heights which decrease from equator towards poles and cirrus clouds can form at very low altitudes (e.g. as low as 3 km in the extreme cold conditions) in the Arctic and high-latitude regions. Therefore, the cloud profiles above 3 km will be considered for further study, which is different from the previous studies in Li and Groß (2021, 2022).

To study the difference of cirrus cloud occurrence and properties in the high- and midlatitude regions, we focus on the area where the CIRRUS-HL field campaign roughly took place in June-July 2021 (e.g. De La Torre Castro et al., 2023) for a potential cross study in the future, i.e. midlatitudes (35–60°N; 30°W–30°E) and high-latitudes (60–80°N; 30°W–30°E). We note that the midlatitudes of this research area covers a large fraction of the North Atlantic flight corridor and hence is strongly influenced by aviation emissions and resulting contrails (e.g. Graf et al., 2012; Schumann and Graf, 2013; Voigt et al., 2017; Urbanek et al., 2018; Li and Groß, 2021, 2022; Groß et al., 2023), whereas the high-latitude regions are more pristine. For the current study, the lidar measurements of CALIPSO in 5 years of 2014 and 2018–2021 are analyzed. The choosing of 2014 is due to the potential cross comparison study between satellite and airborne measurements during the ML-CIRRUS field campaign which took place in March and April, 2014 (Voigt et al., 2017).

3 Differences in cirrus cloud properties across latitudes

3.1 Occurrence rate and geometrical thickness

Following the analysis in a previous study (Li and Groß, 2021) we removed the data either at temperatures above -38°C or with PLDR values falling into the range below 0.10 and above 0.80 to reject as many as possible unphysical signals with large uncertainties. The pre-analyzed observations were further used to infer occurrence rates (ORs) of cirrus clouds as a function of time (here season), latitude, and altitude. To illustrate the variations of ORs along the latitudes, we calculate the profiles of ORs in each 5-degree latitude bin from 35–80°N. The resulting profiles of ORs in different seasons (spring: March–May; summer: June–August; autumn: September–November; winter: December–February) in different years 2014 and 2018–2021 as well as the composite mean values of the 5 years are shown in Figure 1.

All the profiles of ORs in different seasons show a similar feature that is, in general, the occurrence heights of cirrus clouds decrease with increasing latitude (see Figure S1). In spring, for example, the cirrus cloud ORs derived from all the 5-year observations peak at 10.12 km within the latitude bin of 35–40°N while at 7.12 km within 75–80°N and the altitudes at which the maximum ORs are observed vary at 10.66–7.36 km (9.70–6.76 km, 10.60–7.78 km, 9.76–7.30 km, and 10.24–6.64 km) along the latitude bins in 2014 (in 2018–2021, respectively). The altitude ranges in which cirrus clouds formed as well as the altitudes with the maximum ORs in different seasons can be seen in Figure S1 (in the supplementary material). The seasonal

https://doi.org/10.5194/egusphere-2025-2052
Preprint. Discussion started: 19 June 2025

variations in the altitudes with the maximum ORs along the latitudes are discernable, showing the largest values in summer, the smallest in winter, and smaller values in spring than in autumn. The altitude ranges where cirrus clouds form (with a threshold of OR > 1%) generally increase with increasing latitude in both autumn and winter. In spring and summer, however, the ranges only increase with increasing latitude in the midlatitude regions and then decease after the 60°N latitude. Furthermore, there are large variabilities in the altitude ranges of cirrus cloud in different years, especially for those in spring at high-latitudes. A distinct seasonal variation is visible, showing that values of cirrus altitude range varying from 5.5 km (found within 35–40°N in 2021) up to 8 km (found within 55–60°N in 2020) in winter and from 2.7 km to 4.8 km in summer. In spring and autumn, however, the values fall within the range from ∼4.8 to 6.7 km. The details of altitude ranges of cirrus cloud formation (with OR > 1.0%) calculated from all the 5-year observations in different seasons are summarized in Table 1 and a schematic representation can be seen in Figure S1. Furthermore, the ORs of cirrus cloud themselves show a clear seasonal variation with the largest values in winter, the smallest in summer, and larger values in autumn than in spring. These findings are consistent with the results in previous studies (e.g. Sassen et al., 2008; Li and Groß, 2022). The ORs in 2014 are larger than the composite mean values of OR derived from all 5-year observations along the latitudes for all seasons, especially at latitudes from 50°N polewards. These changes in the ORs of cirrus cloud were also indicated in Li and Groß (2022) for a smaller research area at midlatitudes. This is likely due to the fact that air temperatures increased in the past years and even faster at high-latitudes due to AA (e.g. Li and Groß, 2022; Rantanen et al., 2022). To clarify the impacts of meteorological conditions on cirrus cloud formation, we further compare the background temperatures and relative humidity with respect to ice (RHi) directly derived from global ERA-5 re-analysis data (Hersbach et al., 2020) covering the research area in this study (not shown here). Indeed, the temperatures in 2014 are generally lower than in more recent years, especially in the summer months. The RHi values, however, are higher in 2014 than in other years, especially at midlatitudes. Therefore, the meteorological conditions in 2014 are more favorable for ice crystal formation along the latitudes than in the years 2018–2021.

In order to compare the morphologies of cirrus clouds at high-latitudes (HL) and midlatitudes (ML), we divide the data into a subset for HL (60–80°N; 30°W–30°E) and ML (35–60°N; 30°W–30°E) following the commonly-used definitions in previous studies (e.g. De La Torre Castro et al., 2023), although the partitioning of latitude ranges is somehow arbitrary due to lacking of universally-accepted definition of latitude ranges. The composite mean values of cirrus ORs in different seasons calculated from all the 5-year lidar observations in years of 2014 and 2018–2021 are shown in Figure 2. Apparently, cirrus clouds at HL formed mostly at lower altitudes than those at ML due to the fact that favorable atmospheric conditions involving temperature and humidity for ice crystal formation can extend to lower altitudes at HL. The differences between the altitudes at which the maximum ORs are observed at HL and ML show a distinct seasonal dependence. For example, the height difference of maximum ORs is 1.77 km in winter but is only 1.14 km in summer. The heights of cirrus cloud formation typically range from near 7.0 to 12.0 km (5.0–12.5 km) for HL and 7.8 to 13.2 km (6.0–13.5 km) for ML in summer (in other seasons). The cloud tops of cirrus are very similar in different seasons (roughly 12.5 km at HL and 13.5 km at ML) whereas the cloud bottoms are much higher in summer than in other seasons. In addition, the values of OR show much larger variabilities at HL than at ML, which is related to the larger variabilities in humidity at HL than at ML and is consistent with a recent model study showing larger INP effects on cirrus at higher latitudes (Beer et al., 2024). The ORs of cirrus cloud at HL can get as large as

https://doi.org/10.5194/egusphere-2025-2052
Preprint. Discussion started: 19 June 2025

Table 1. Altitude range of cirrus clouds calculated from the composite 5-year observations in different seasons with ORs larger than 1.0%.

Latitude (°N)	35–40	40–45	45–50	50–55	55–60	60–65	65–70	70–75	75–80
MAM (km)	5.40	5.61	5.52	5.70	6.06	6.06	6.03	5.94	5.79
JJA (km)	3.18	4.08	4.38	4.50	4.50	4.35	3.99	3.48	3.36
SON (km)	5.16	5.55	5.64	5.82	5.97	5.94	6.12	6.21	6.39
DJF (km)	5.91	6.57	6.99	7.20	7.05	7.20	7.38	7.23	7.14

15.03% at 7.90 km in winter but only 5.24% at 9.10 km in summer. At ML, however, the maximum ORs are within the range from 7.10% to 10.81%.

We next analyze the geometrical thickness of cirrus cloud, which is defined as the vertical distribution of cirrus clouds at different latitudes (e.g. Li and Groß, 2021). According to the definitions with cloud thickness larger than 0.1, 0.3, 1.0, and 2.0 km, respectively, the relative probabilities of the occurrence in different seasons at HL and ML are hence calculated and shown in Figure 3. First, there is a distinct seasonal cycle in the geometrical thickness of cirrus clouds with the largest values in winter and the smallest in summer for both HL and ML and for all the thickness thresholds. In addition, the comparisons of cloud thickness in different seasons show that the thickest cirrus clouds formed in winter and the thinnest ones in summer. The cloud thickness at ML are very close to each other in spring and autumn whereas at HL they are thinner in spring than in autumn. Comparisons in different seasons show that the cloud thicknesses in spring and summer (in autumn and winter) are thicker (thinner) at ML than at HL. Therefore, there are larger variabilities in cloud thickness at HL than ML in all seasons, which is presumed to be caused by the larger variabilities in the humidity (RHi) and lower air temperatures at HL than ML (not shown here) as well as the larger INP effects on cirrus at higher latitudes (e.g. Beer et al., 2024). The results in different years show remarkable reductions in cirrus thickness only at ML in spring and summer of 2020–2021 and in winter of 2021, which is very well following the timeline of the aviation reduction during the COVID-19 pandemic (e.g. Li and Groß, 2021). The changes in cloud thickness induced by the aviation reduction are presumed to be smaller at HL than ML since the HL regions are much more pristine and are subjected to the larger variabilities of cirrus clouds at HL. In addition, we also compare the monthly geometrical thicknesses of cirrus clouds at ML and HL (not shown here). The results show that there are stronger seasonal variations in the geometrical thickness of cirrus at HL than ML. For the cases with the definition of cloud thickness larger than 0.3 km, for example, cirrus clouds at HL reached the maximum frequency of 39.29% in January and the minimum frequency of 13.46% in June whereas at ML they reached the extremes of 32.10% in December and 15.52% in July, respectively. Further, the values are very similar at HL and ML in April and August and become smaller at HL than ML in the warmer months (May–July) and larger at HL than ML in the colder months (September–March).

3.2 Extinction coefficient and effective optical depth

The extinction coefficient of ice crystals in cirrus quantifies the rate of decrease in the intensity of light (at 532 nm in this study), which accounts for the absorption and scattering of light by ice crystals. It is influenced by several microphysical properties of

https://doi.org/10.5194/egusphere-2025-2052
Preprint. Discussion started: 19 June 2025

ice crystals, including particle size distribution, shape, orientation, and complexity as well as their optical properties (such as refractive index and absorption coefficient).

The CALIOP datasets used here provide profiles of particulate volume extinction coefficient. The retrieval algorithms of extinction coefficient profiles are described by Vaughan et al. (2009) by exploiting the total backscatter measurements in combination with the particulate lidar ratio from the CALIOP raw data. The lidar ratio for ice clouds is considered to be constant over certain intervals within each backscatter profile and is determined by applying an empirical linear function of mid-cloud temperature developed by Platt et al. (1998, 2002). Due to the temperature-dependent IWC-extinction relationship, IWC is calculated as a parameterized function of the retrieved extinction coefficients within ice crystals of cirrus clouds involving temperature and effective diameter of ice crystals and is stored in the Level 2 cloud profile product (Heymsfield et al., 2005; Mioche et al., 2010; Heymsfield et al., 2014). In the current study, we only compare the profiles and distributions of extinction coefficients of ice crystals at HL and ML.

The resulting vertical profiles of cirrus extinction medians in spring (MAM: March–May) are shown in Figure 4 (left panel). In general, they reveal a decrease with increasing altitude for all the cases in different years and in different latitude ranges (i.e. at HL and ML, respectively), indicating smaller and fewer ice crystals at higher altitudes. Besides the differences in the altitudes containing cirrus cloud formation (with ORs > 1.0%) at different latitudes (with nearly 1.5-km discrepancy; See more descriptions in details in Subsection 3.1), cirrus clouds probed at HL are characterized with smaller extinction coefficients than those at ML (e.g. Gasparini et al., 2018). This is closely linked to the dominant formation processes of ice crystals depending on temperature and relative humidity over ice (RHi). While liquid-origin cirrus clouds dominate at relatively warmer and moister midlatitudes via heterogeneous nucleation, in situ-formed cirrus clouds dominate at colder and drier air masses prone to occurring at high latitudes (Gasparini et al., 2018). Further, the differences between cirrus extinction coefficients at HL and ML become smaller with increasing altitudes from 0.14 to 0.03 km^{-1} derived from the composite values of 5-year observations.

To compare the cirrus extinction coefficients at different latitude ranges, we show box plots in the right panel of Figure 4 for the extinction coefficient distributions in spring in different years of 2014 and 2018–2021. At ML, the year-to-year variations in extinction coefficients are discernable with a slight increase from 2014 to 2019 with the medians from 0.175 to 0.205 km^{-1} and with notable reductions in 2020 and 2021 with the medians of 0.169 and 0.160 km^{-1}, respectively, which might be partially related to the aviation reduction during the COVID-19 period. However, the influences of variable meteorological conditions cannot be ruled out (e.g. Schumann et al., 2021a; *Quaas et al.*, 2021; Li and Groß, 2021). At HL, however, extinction coefficients are comparable in different years with an exception of a small enhancement in 2019 with medians from 0.131 to 0.146 km^{-1}. The comparison of extinction coefficient distributions across latitudes shows a clear consistence in different years, i.e. the extinction coefficients are larger at ML than at HL. From the composite values in 5 years, the extinction coefficients are within the range of 0.012 to 1.284 km^{-1} (considering the 5% to 95% percentile of the data set) at ML and from 0.010 to 1.005 km^{-1} at HL, respectively. The distributions of extinction coefficients in other seasons are also shown in Figure S2. From Figure S2 (Panels a, b, d, e), the seasonality in extinction coefficient distributions is noticeable, showing the largest extinction coefficients in winter and the smallest in summer. In addition, the latitudinal comparison shows a stronger seasonal variation at

https://doi.org/10.5194/egusphere-2025-2052
Preprint. Discussion started: 19 June 2025

HL than at ML. Considering the impact of polar day and night, we also show the results only from the day-time measurements in summer (Panel S2c) and only from the night-time measurements in winter (Panel S2f) for a fair comparison between HL and ML. In general, the diurnal variations of extinction coefficient are notable, which show larger values during day time than night time for both seasons (the same diurnal variations are also seen in spring and autumn). And further, the diurnal variations are stronger at ML than at HL, which backs up the necessity of considering the impacts of polar day and night. Furthermore, the year-to-year variations are stronger in autumn and winter than in spring and summer for both latitude ranges. In particular, extinction coefficients during the COVID-19 pandemic are in general smaller than those in the other non-COVID years at ML, whereas at HL, the reductions in extinction coefficient cannot be clearly recognized.

Effective optical depth of cirrus clouds is a good measure to quantify the overall impact of cirrus clouds on the absorption and scattering of light passing through the cloud. Previous studies indicated that cirrus is the only cloud genus capable of inducing either cooling or heating during daytime at the top of the atmosphere (TOA) and the radiative balance greatly depends on their optical depth (Lolli et al., 2017; Campbell et al., 2016, 2021). Although studies on the cloud optical depth of cirrus have been carried out intensively, investigations of its geometrical and optical properties over the Arctic are still rare. According to Equation 1, the effective optical depths of cirrus clouds are calculated as the integral of the extinction over the altitudes of the vertical distributions of cirrus. The resulting histograms of effective optical depth, for example, in spring in different years of 2014 and 2018–2021 are shown in Figure 5. First, the histograms of cirrus effective optical depths exhibit a left-skewed distribution with a long tail extending to smaller values other than a normal distribution in the logarithmic scales. cirrus clouds at ML are characterized with slightly larger effective optical depth than at HL. That is, the values derived from the composite data of the 5 years are within the ranges from ∼0.005 to 1.258 (again from 5% to 95% percentile of the data set) for cirrus clouds at HL and from ∼0.004 to 1.373 at ML. We also note that both the threshold values are smaller in 2020 and 2021 than in other years for both HL and ML. Furthermore, the corresponding medians for different years consistently show larger values at ML than HL with a difference of 0.015 from the composite data of the 5 years. Please note the deviation of medians in 2020 from those of other years which might be correlated with the late phase of anomalies in the Arctic polar vortex in 2019/2020 (e.g. Lawrence et al., 2020; Huang et al., 2021), which could increase the optical depth of cirrus by lifting moist air into higher and colder altitudes to enhance the formation of smaller ice crystals. Indeed, the meteorological conditions derived from the ERA5-reanalysis data reveal lower temperatures and enhanced RHi in the spring months in 2020 than in other years (not shown here). In addition, seasonal variations in effective optical depth of cirrus clouds are also noticeable with the largest values in winter and the smallest in summer (see Figures S3-S5 for the histograms of effective optical depth in other seasons). The differences in effective optical depth across latitudes (i.e. larger values at ML than at HL) are more notable in spring and summer than in autumn. In winter, however, the values are similar between different latitudes.

3.3 Particle linear depolarization ratio

As mentioned above the CALIOP lidar is polarization-sensitive at 532 nm and is able to independently measure two orthogonal polarization components which are polarized parallel and perpendicular to the polarization plane of the transmitted beam. Thus,

https://doi.org/10.5194/egusphere-2025-2052
Preprint. Discussion started: 19 June 2025

the Level 2 cloud profile products also contain the information of particle linear depolarization ratio (PLDR). We next turn to compare the distributions of PLDR in different years across latitudes.

In Figure 6, we present the distributions of cirrus PLDR in box plots for each 5-degree latitude bin in spring (Mar–May) derived from both day- and night-time observations from years of 2014 and 2018–2021 as well as from the composite values of 5 years. For all the cases, the mean values of PLDR are larger than the corresponding medians, implying that the PLDR values follow a positively-skewed distribution (e.g. Li and Groß, 2021). The year-to-year variabilities in PLDR show larger values in the non-COVID years (2014, 2018, and 2019) than in 2020 and 2021 under the aviation reduction during the COVID-19 pandemic at midlatitudes (ML) (e.g. Li and Groß, 2021). At high-latitudes (HL), however, the PLDR values decrease with increasing latitude only in 2014 and 2018 and become nearly constant in 2019 and 2021. The case in 2020 is distinctive from other years, showing that PLDR tend to slightly increase with increasing latitude (only at latitudes larger than 60°N). This leads to the comparable values in the PLDR distribution at ML and HL because of the reduction in PLDR at ML caused by the aviation reduction due to the COVID-19 restriction (Li and Groß, 2021) and additionally of enhancement in PLDR at HL in connection with the unusual strong stratospheric polar vortex (e.g. Lawrence et al., 2020; Huang et al., 2021). The corresponding results in other seasons are indicated in Figures S6-S8 in the supplementary material, which present similar characteristics as the PLDR analysis in spring. Besides the year-to-year variabilities, the composite values of cirrus PLDR of the 5 years show a clear decrease with increasing latitude for all the seasons. As a summary, we provide the quartiles (Q1, Q2, and Q3 = 25th, 50th, and 75th percentiles, respectively) of all the PLDR values from the composite 5-year observations in spring in Table 2.

We next compare the PLDR distributions of cirrus clouds in different seasons at HL and ML, respectively, in more detail in Figure 7. Besides the seasonality, PLDR are generally larger at ML than at HL, especially in spring and autumn. The only exception is spring 2020 with slightly larger PLDR at HL than at ML, as mentioned before. Similarly, the enhancements in PLDR at HL are also seen in autumn 2019 and winter 2019/2020 compared to the corresponding seasons in other years. The reasons for the enhanced PLDR at HL are presumed to relate to lower temperatures as well as higher aerosol loading (including soot and smoke) caused by the long-lasting strong stratospheric polar vortex during this period (e.g. Manney et al., 2022; Ansmann et al., 2023). Besides the reductions in PLDR at ML during the COVID-19 restriction, the values of PLDR at ML are relatively stable, showing small year-to-year variabilities. In contrast, the year-to-year variabilities in PLDR at HL are much larger in all seasons. The impacts of the COVID-19 on the cirrus cloud properties at HL are difficult to identify since the potential COVID-induced changes in PLDR are too small and are obscured by the large year-to-year variabilities. We note that the lidar measurements at HL in summer are mostly derived during daytime (polar day) and, in contrast, the measurements at HL in winter are mostly at night (polar night). Previous studies reveal that aviation exerts a stronger influence on cirrus cloud properties in the daytime than at night (e.g. Graf et al., 2012; Schumann and Graf, 2013; Li and Groß, 2022). Therefore, we also derive the results from only the daytime measurements in the summer months and from only the night-time measurements in winter at ML and HL for a fair comparison. The resulting distributions of cirrus PLDR are shown in the Panels c and f of Figure 7. Diurnal variations in PLDR are remarkable, showing larger values during daytime than at night (e.g. Sassen and Zhu, 2009; Li and Groß, 2022). For the comparison during daytime in summer, the difference of PLDR between

https://doi.org/10.5194/egusphere-2025-2052
Preprint. Discussion started: 19 June 2025

Table 2. The quartiles of all the PLDR values from the composite 5-year observations in spring (Mar–May) within the altitudes 6–12 km.

Latitude (°N)	35–40	40–45	45–50	50–55	55–60	60–65	65–70	70–75	75–80
Q1	0.2658	0.2612	0.2524	0.2466	0.2436	0.2395	0.2418	0.2362	0.2374
Q2	0.3646	0.3613	0.3533	0.3466	0.3418	0.3352	0.3386	0.3322	0.3358
Q3	0.4720	0.4708	0.4676	0.4628	0.4578	0.4510	0.4559	0.4522	0.4577

ML and HL becomes much larger than the results derived from both day- and night-time observations. However, the night-time measurements in winter (Panel f) show the opposite, namely the differences in PLDR across latitudes become smaller compared with the results from both day- and night-time observations. The findings are backed up by the fact that aviation densities are larger during daytime than at night (e.g. Graf et al., 2012; Schumann and Graf, 2013).

4 Discussion

4.1 Implications of previous studies

Although the current understanding of cirrus cloud properties has been improved with theoretical and experimental efforts over the last decades, there are still many remaining uncertainties, especially the impacts of aviation emissions. To our knowledge, Urbanek et al. (2018) is one of the first studies to show the potential effect of aviation emissions on cirrus cloud properties. With airborne lidar measurements through specific clouds, they indicated that enhanced heterogeneous freezing on aviation exhaust particles is responsible for the resulting lower supersaturation and larger particle linear depolarization ratios (PLDR) (Urbanek et al., 2018). The findings were further backed up by the satellite measurements with CALIPSO. Namely, the aviation-induced changes in cirrus cloud properties can be characterized by the distributions of cirrus PLDR either during a specific period with a strong aviation reduction due to the COVID-19 pandemic or during a 10-year term with a slight increase in aviation emissions (Li and Groß, 2021, 2022).

4.2 Ambient temperatures in the high- and midlatitude regions

Our analysis above shows that, besides seasonality, there are significant deviations in the occurrence rates (OR) and optical properties of cirrus clouds forming at different latitudes. Since the background meteorological conditions (including temperature, humidity, and dynamics) play a crucial role in the formation and evolution of cirrus clouds, we exam the relationship between cirrus cloud properties and the ambient temperatures inside cirrus clouds.

Previous studies reveal that cirrus cloud formation and morphologies as well as the high degree of variability in their microphysical properties strongly depend on the background meteorological conditions, especially on temperatures (Urbanek et al., 2018; Li and Groß, 2021). A direct comparison between PLDR and the ambient temperatures showed that the PLDR values decrease with rising temperatures at temperatures below -50°C and become stable at warmer temperatures higher than -50°C

https://doi.org/10.5194/egusphere-2025-2052
Preprint. Discussion started: 19 June 2025

(Li and Groß, 2021). These findings help to interpret the potential causes for the latitudinal differences of cirrus cloud properties. The datasets of temperature used here are derived from the GEOS-5 (Goddard Earth Observing System, version 5) model data product provided to CALIPSO by the Global Modeling and Assimilation Office (GMAO) data assimilation system.

Figure 8 shows the histograms of temperature inside cirrus clouds in spring of different years at HL and ML, respectively. The distributions show a clear consistence in different years at both latitude ranges. The cirrus cloud formation at ML took place with the maximum occurrence at temperature of -38°C, the temperature mask we chose to filter out aerosols and non-cirrus clouds from the dataset, and with a "shoulder" as temperature reached ∼-60°C. Cirrus clouds at HL, however, occurred at temperatures following a quasi-lognormal distribution with peaks at ∼-45°C with a cutoff at -38°C due to the temperature filtering. For both cases, the histograms of temperatures inside cirrus clouds can be characterized by a left-skewed distribution with a long tail extending to lower temperatures. The comparisons between different latitudes show larger medians at ML than HL by nearly ∼1°C in 2014, 2018, and 2019, and nearly identical medians in 2021. The case in 2020 shows smaller medians at ML than HL by 1.5°C and the histograms at HL with a longer tail extending to -76.22°C, which is related to the lower temperatures caused by the strong stratospheric polar vortex lasting from autumn 2019 to spring 2020. Regarding all 5-year measurements, the values are very close across latitudes in terms of the medians and statistical distributions. For the 5-year measurements in other seasons (see Figures S9-S11), the medians of temperatures inside cirrus clouds are larger at ML than HL by 3.1 and 1.6°C in summer and autumn, respectively, but smaller at ML than HL by 1.6°C in winter. Based on these comparisons, we may conclude that temperatures inside cirrus clouds can likely be excluded as the cause for the difference in the cirrus extinction and PLDR at different latitudes as shown in the present study.

4.3 Aerosol loading and aviation emissions in the high- and midlatitude regions

As mentioned above the research area in this study covers a large portion of the northern hemisphere spanning from the northern Atlantic to the European mainland and extending into the Arctic. It is characterized by a large diversity of geography, climate, and environment including a wide range of aerosol types. The presence of aerosol particles in the atmosphere can catalyze the formation of ice crystals by aerosols acting as ice-nucleating particles (INPs) which induce heterogeneous freezing at sub-zero temperatures > -38°C and lower supersaturations with respect to ice compared to homogeneous freezing (Koop et al., 2000; Hoose and Möhler, 2012). With the airborne lidar measurements of WALES, Urbanek et al. (2018) indicated that the increased heterogeneous freezing caused by aviation emissions can be responsible for the enhanced PLDR of cirrus clouds. The finding is further supported by the microphysical properties of the high-PLDR-mode cirrus clouds, which exhibit larger effective ice particles and lower number concentrations confirming the effects of enhanced heterogeneous freezing (Groß et al., 2023).

The tiny aerosol particles suspended in air vary widely in type and composition, which leads to significant variations in the microphysics of ice clouds and further influences their optical and radiative properties and climate effects (Boucher et al., 2013). However, INP concentrations are typically very low in the atmosphere, with only a tiny fraction of 10^{-3} to 10^{-5} of the ambient aerosols acting as INPs (Rogers et al., 1998) and even a lower fraction in marine regions (Rosinski and Morgan, 1988). INPs can be natural or anthropogenic particles, originating from dust storms, volcanic eruptions, sea spray, biogenic emissions, and anthropogenic activities (including industrial emissions, vehicle exhaust, and urban pollution) (Hoose and Möh-

https://doi.org/10.5194/egusphere-2025-2052
Preprint. Discussion started: 19 June 2025

ler, 2012; Kulkarni et al., 2016; Kärcher, 2017; Kanji et al., 2017; Gao et al., 2022; Beer et al., 2022, 2024). The distribution of aerosol particles in the high-latitude and midlatitude regions can vary significantly due to the differences in their sources. At midlatitudes, aerosol types are predominantly sulfates, black carbon and organic carbon with anthropogenic sources as well as mineral dust and sea salt from natural emissions; whereas at high-latitudes, in contrast, the overall aerosol concentrations are lower with more natural aerosols including sea salt (mostly at lower levels), biogenic particles, and wildfire smoke. Nevertheless, the aerosol types and compositions across latitudes can influence each other due to transport mechanisms and atmospheric circulation patterns. According to recent model simulations (Beer et al., 2022, 2024), mineral dust and black carbon that are commonly considered as the main INP types in global models show a distinct north-south gradient with larger concentrations at midlatitudes than high-latitudes.

In addition, soot particles from aviation emissions are presumed to play a determinate role in the formation of contrails and contrail cirrus, since aviation exhaust particles are mainly emitted at cirrus cloud altitudes leading to aviation soot number concentrations at flight altitude often exceeding those of other aerosols (Righi et al., 2021). While soot particles from modern aircraft engines may not be highly efficient INPs for direct ice crystal formation at cirrus temperatures (Testa et al., 2024a, b; Yu et al., 2024), they still play a crucial role in the formation of contrails and further evolving into contrail cirrus (Chauvigné et al., 2018), especially at midlatitudes with heavy air traffic. However, cirrus cloud formation is very complex depending on atmospheric conditions of temperature, humidity, vertical motion and other coexistent aerosols. Furthermore, soot particles may undergo multiple cloud cycles during their residence time in the atmosphere, which can improve their porosity and surface wettability and thus change their ability for pore condensation and freezing (PCF) (e.g. Mahrt et al., 2018; Gao et al., 2022). In addition, previous studies indicated that soot particles involved in ice crystal formation may lead to more irregular ice crystal shapes in cirrus cloud depending on their surface features and chemical compositions (Kärcher and Lohmann, 2003; Hoose and Möhler, 2012), which is responsible for the enhanced PLDR of cirrus clouds (Urbanek et al., 2018; Li and Groß, 2021, 2022). Due to various factors including population distribution, social and economic activities, and geographical constrains, aviation densities at midlatitudes are much larger than at high-latitudes (by a factor of more than 10 times) (Stettler et al., 2013; Teoh et al., 2024).

5 Conclusions

In the last decades, the Arctic has been warming at a faster rate compared to the global average, which is known as Arctic amplification (AA). The thin cirrus clouds in the Arctic that exert a substantial positive forcing on the surface temperatures can trigger AA and further accelerate the processes of warming, especially in polar winter. Compared to the intensive studies of cirrus clouds in the tropics and midlatitude regions, however, direct measurements and model simulations at high-latitudes are still very rare. In the current paper, we present an analysis of cirrus clouds from midlatitudes (ML, 35–60°N; 30°W–30°E) towards high-latitudes (HL, 60–80°N; 30°W–30°E) with lidar measurements of CALIPSO in the years 2014 and 2018–2021. The derived occurrence and properties of cirrus clouds have been compared across latitudes.

https://doi.org/10.5194/egusphere-2025-2052
Preprint. Discussion started: 19 June 2025

The resulting profiles of occurrence rates (ORs) of cirrus clouds in different seasons follow a distinct seasonal cycle with the largest values in winter, the smallest in summer, and larger values in autumn than in spring. The seasonal cycles in ORs at HL are much stronger than at ML with nearly 10% difference of ORs at HL compared to only 3.7% at ML. Furthermore, the heights of cirrus cloud formation show a clear decrease with latitudes. Depending on the meteorological conditions for ice crystal formation, cirrus clouds in summer only appear at higher altitudes compared to other seasons, which results in similar cloud tops in all seasons but much higher cloud bottoms in summer than in other seasons. The geometrical thicknesses of cirrus clouds defined as the vertical extension of cirrus at different latitudes also show a distinct seasonal cycle with the largest values in winter and the smallest in summer at both HL and ML and for all analyzed thickness thresholds. The seasonality at HL is stronger than at ML. Furthermore, the cloud thicknesses are also compared across latitudes and show larger (smaller) values at ML in spring and summer (in autumn and winter) than at HL.

We next compare the extinction coefficients of cirrus clouds and their vertical profiles show a decrease with increasing altitude in different years within both HL and ML regions. Besides the 1.5-km differences in the altitudes of cirrus cloud formation at different latitudes in spring, cirrus clouds observed at HL are characterized with smaller extinctions than those at ML. The differences in extinctions at different latitudes may be connected to the nucleation processes of ice crystals depending on the meteorological conditions and the availability of INPs. Notably, the year-to-year variations in extinctions show a slight increase from 2014 to 2019 and a notable reduction in 2020 and 2021 at ML while staying nearly identical in different years at HL. Further, they are stronger in autumn and winter than in other seasons for both HL and ML. In addition, the seasonal variations in extinction show the largest values in winter and the smallest in summer, which are stronger at HL than at ML. We notice that cirrus cloud extinctions during the COVID-19 pandemic (starting from spring 2020) are in general smaller than those in the non-COVID years at ML, whereas there are no clear reductions in extinctions being recognized at HL. The effective optical depths of cirrus show, in general, the same seasonality as extinctions with larger values at ML than at HL except for the winter months.

Particle linear depolarization ratios (PLDR) decrease with increasing latitude, considering the mean over all analyzed years. However, the characteristics of PLDR distributions vary in different years. The year-to-year variabilities in PLDR show larger values in the non-COVID years (2014, 2018, and 2019) than in 2020 and 2021 possibly influenced by aviation reductions during the COVID-19 pandemic at ML. At HL, however, PLDR show no clear reductions during the same period of COVID-19. This is likely a result of reduced air traffic at HL and potential smaller aviation effects in that regions being masked by the large year-to-year variabilities.

To study the potential causes for the latitudinal differences in cirrus cloud properties, we first determine the distributions of temperatures inside cirrus clouds at different latitudes. Their histograms show a similar distribution in different years at both HL and ML, following a left-skewed distribution with a long tail extending to lower values. At ML, cirrus clouds mainly formed within the temperature range from -60° to -38° with the maximum occurrence at -38°. At HL, however, the temperatures inside cirrus follow a quasi-lognormal distribution with a cutoff at -38°, peaking at ∼-45°. In spring, temperatures inside cirrus are characterized with larger medians at ML than at HL in 2014, 2018, and 2019, smaller medians at ML than at HL in 2020, and nearly identical medians in 2021. In other seasons, however, the medians of temperatures inside cirrus across latitudes

https://doi.org/10.5194/egusphere-2025-2052
Preprint. Discussion started: 19 June 2025

vary slightly with differences up to ∼3°C determined from the composite values of 5-year measurements. Due to the weak latitudinal dependency, temperatures within cirrus clouds are likely not the cause of the latitudinal differences in cirrus cloud properties shown here.

Finally, we compare aerosol concentrations at different latitudes, as reported in previous studies, which can act as ice-nucleating particles (INPs) to form ice crystals via heterogeneous freezing. The distribution of aerosol particles across latitudes can vary significantly due to the different sources of these particles, i.e. with higher aerosol concentrations from more anthropogenic sources at ML and lower concentrations with more natural aerosols at HL. Although transport mechanisms and atmospheric processing may influence the aerosol compositions and concentrations at different latitudes, there is a distinct north–south gradient in the number concentrations of dust and soot with larger values at ML than at HL. In addition, aviation-induced soot particles that are more significant at ML than at HL are emitted directly into the cirrus regime and could often show larger concentrations compared to other aerosols at aviation cruising altitudes. Although soot particles from modern aircraft engines may not be efficient INPs (Testa et al., 2024a, b; Yu et al., 2024), they can act as condensation nuclei for forming tiny water droplets, especially, as they aggregate and mix with other substances. These processes will influence ice cloud formation indirectly by competing with other aerosols for available water vapor and suppressing homogeneous nucleation. Furthermore, soot particles play a crucial role in the formation of contrails and contrail-cirrus. They may undergo multiple cloud cycles during their residence time in the atmosphere and thus improve their ice-nucleating ability via PCF. Notably, ice crystals forming through heterogeneous freezing are characterized by larger sizes and more irregular shapes. In turn we hypothesize that the differences between heterogeneous and homogeneous freezing depending on latitudes may be responsible for the observed latitudinal dependency of cirrus cloud properties. This work highlights the differences in the optical properties of cirrus cloud across latitudes that is crucial for improving global climate models and understanding the important role cirrus clouds play in Earth's radiation budget and climate feedback. However, CALIOP suffers in several limitations such as low signal-to-noise ratio, daytime limitation, low sampling resolution, etc. In the future work, we will make use of the lidar measurements with the Atmospheric Lidar (ATLID) onboard EarthCARE which is a linearly polarized, high-spectral-resolution lidar (HSRL) system and represents a significant advancement in spaceborne lidar technology for studying cirrus clouds (Wehr et al., 2023). It allows us further to compare the cirrus cloud properties with the vertical updrafts and ambient aerosol loading.

Code availability. Data description and example codes for handling the VFM data are available at https://asdc.larc.nasa.gov/ (NASA, 2025a). The MATLAB codes for drawing the plots in this paper are available from Zenodo at https://doi.org/10.5281/zenodo.15063832.

Data availability. The CALIPSO data, including VFM used in this study, can be obtained via https://subset.larc.nasa.gov/calipso/login.php (NASA, 2025b, login required). The reanalyzed data of cirrus parameters in different month in the years 2014 and 2018–2021 are available from Zenodo at https://doi.org/10.5281/zenodo.15063832.

https://doi.org/10.5194/egusphere-2025-2052
Preprint. Discussion started: 19 June 2025

Author contributions. QL collected and analyzed the data and wrote the manuscript with help from SG. Both authors discussed the results and findings and contributed to finalizing the manuscript.

Competing interests. The authors declare that they have no conflict of interest.

Acknowledgements. This project has received funding from Horizon Europe programme under Grant Agreement No 101137680 via project CERTAINTY (Cloud-aERosol inTeractions & their impActs IN The earth sYstem). Furthermore, this research has been supported by the DLR internal funding within the MABAK project (Innovative Methoden zur Analyse und Bewertung von Veränderungen der Atmosphäre und des Klimasystems). We thank the NASA Langley Research Center Atmospheric Science Data Center (ASDC) and CALIPSO science team for making the data available for research. This paper has greatly benefited from an internal review by Christof Beer (DLR, Germany).

https://doi.org/10.5194/egusphere-2025-2052
Preprint. Discussion started: 19 June 2025

References

Ansmann, A., Ohneiser, K., Engelmann, R., Radenz, M., Griesche, H., Hofer, J., Althausen, D., Creamean, J. M., Boyer, M. C., Knopf, D. A., Dahlke, S., Maturilli, M., Gebauer, H., Bühl, J., Jimenez, C., Seifert, P., and Wandinger, U.: Annual cycle of aerosol properties over the central Arctic during MOSAiC 2019–2020 – light-extinction, CCN, and INP levels from the boundary layer to the tropopause, Atmos. Chem. Phys., 23, 12821–12849, https://doi.org/10.5194/acp-23-12821-2023, 2023.

Bailey, M. P. and Hallett, J.: Growth rates and habits of ice crystals between -20°C and -70°C, J. Atmos. Sci., 61), 514–554, 2004.

Bailey, M. P. and Hallett, J.: A comprehensive habit diagram for atmospheric ice crystals: Confirmation from the laboratory, AIRS II, and other field studies, J. Atmos. Sci., 66, 2888–2899, https://doi.org/10.1175/2009JAS2883.1, 2009.

Baran, A. J.: A review of the light scattering properties of cirrus, J. Quant. Spectrosc. Radiat. Transfer, 110 (14-16), 1239 –1260, https://doi.org/10.1016/j.jqsrt.2009.02.026, 2009.

Beer, C. G., Hendricks, J., and Righi, M.: A global climatology of ice-nucleating particles under cirrus conditions derived from model simulations with MADE3 in EMAC, Atmos. Chem. Phys., 22, 15887–15907, https://doi.org/10.5194/acp-22-15887-2022, 2022.

Beer, C. G., Hendricks, J., and Righi, M.: Impacts of ice-nucleating particles on cirrus clouds and radiation derived from global model simulations with MADE3 in EMAC, Atmos. Chem. Phys., 24, 3217–3240, https://doi.org/10.5194/acp-24-3217-2024, 2024.

Boucher, O., Randall, D., Artaxo, P., Bretherton, C., Feingold, G., Forster, P., Kerminen, V.-M., Kondo, Y., Liao, H., Lohmann, U., Rasch, P., Satheesh, S. K., Sherwood, S., Stevens, B., and Zhang, X. Y.: Clouds and Aerosols. In: Climate Change 2013: The Physical Science Basis, Contribution of Working Group I to the Fifth Assessment Report of the Intergovernmental Panel on Climate Change, edited by: Stocker, T. F., Qin, D., Plattner, G.-K., Tignor, M., Allen, S. K., Boschung, J., Nauels, A., Xia, Y., Bex, V., and Midgley, P. M., Cambridge University Press, Cambridge, United Kingdom and New York, NY, USA, 571–657, 2013.

Bock, L, and Burkhardt, U.: Contrail cirrus radiative forcing for future air traffic, Atmos. Chem. Phys., 19, 8163–8174, https://doi.org/10.5194/acp-19-8163-2019, 2019.

Burkhardt, U., and Kärcher, B.: Global radiative forcing from contrail cirrus, Nat. Clim. Change, 1, 54–58, https://doi.org/10.1038/nclimate1068, 2011.

Campbell, J. R., Lolli, S., Lewis, J. R., Gu, Y., and Welton E. J.: Daytime cirrus cloud top-of-the-Atmosphere radiative forcing properties at a midlatitude site and their global consequences, J. Appl. Meteor. Climatol., 55(8), 1667–1679, https://doi.org/10.1175/JAMC-D-15-0217.1, 2016.

Campbell, J.R., Dolinar, E.K., Lolli, S., Fochesatto, G.J., Gu, Y., Lewis, J.R., Marquis, J.W., McHardy, T.M., Ryglicki, D.R., Welton, E.J.: Cirrus cloud top-of-the-atmosphere net daytime forcing in the Alaskan subarctic from ground-based MPLNET monitoring. J. Appl. Meteorol. Climatol., 60, 51–63, https://doi.org/10.1175/JAMC-D-20-0077.1, 2021.

Chauvigné, A., Jourdan, O., Schwarzenboeck, A., Gourbeyre, C., Gayet, J. F., Voigt, C., Schlager, H., Kaufmann, S., Borrmann, S., Molleker, S., Minikin, A., Jurkat, T., and Schumann, U.: Statistical analysis of contrail to cirrus evolution during the Contrail and Cirrus Experiment (CONCERT), Atmos. Chem. Phys., 18, 9803–9822, https://doi.org/10.5194/acp-18-9803-2018, 2018.

Chen, J., Rossow, W. B., and Zhang, Y.: Radiative effects of cloud-type variations, J. Climate, 13, 264–286, https://doi.org/10.1175/1520-0442(2000)013<0264:REOCTV>2.0.CO;2, 2000.

Corti, T. and Peter, T.: A simple model for cloud radiative forcing, Atmos. Chem. Phys., 9, 5751–5758, https://doi.org/10.5194/acp-9-5751-2009, 2009.

https://doi.org/10.5194/egusphere-2025-2052
Preprint. Discussion started: 19 June 2025

Dai, A., and Deng, J.: Arctic amplification weakens the variability of daily temperatures over northern middle-high latitudes, J. Climate, 34(7), 2591–2609, https://doi.org/10.1175/JCLI-D-20-0514.1, 2021.

De La Torre Castro, E., Jurkat-Witschas, T., Afchine, A., Grewe, V., Hahn, V., Kirschler, S., Krämer, M., Lucke, J., Spelten, N., Wernli, H., Zöger, M., and Voigt, C.: Differences in microphysical properties of cirrus at high and mid-latitudes, 23, 13167–13189, https://doi.org/10.5194/acp-23-13167-2023, 2023.

DeMott, P. J., Sassen, K., Poellot, M. R., Baumgardner, D., Rogers, D.C., Brooks, S. D., Prenni, A. J., Kreidenweis, S. M.: African dust aerosols as atmospheric ice nuclei, Geophys. Res. Lett., 30, 1732, https://doi.org/10.1029/2003GL017410, 2003.

England, M. R., Eisenman, I., Lutsko, N. J., and Wagner, T. J.: The recent emergence of Arctic Amplification. Geophys. Res. Lett. 48, https://doi.org/10.1029/2021GL094086, 2021.

Fletcher, J., Mason, S., and Jakob, C.: The Climatology, Meteorology, and Boundary Layer Structure of Marine Cold Air Outbreaks in Both Hemispheres, J. Climate, 29, 1999–2014, https://doi.org/10.1175/JCLI-D-15-0268.1, 2016.

Francis, J. A., and Vavrus, S. J.: Evidence linking Arctic amplification to extreme weather in mid-latitudes, Geophys. Res. Lett., 39, L06801, doi:10.1029/2012GL051000, 2012.

Freudenthaler, V., Esselborn, M., Wiegner, M., Heese, B., Tesche, M., Ansmann, A., Müller, D., Althause, D., Wirth, M., Fix, A., Ehret, G., Knippertz, P., Toledano, C., Gasteiger, J., Garhammer, M., Seefeldner, M.: Depolarization ratio profiling at several wavelengths in pure Saharan dust during SAMUM 2006, Tellus, 61B, 165–179, 2009.

Fu, Q., and Liou, K. N.: Parameterization of the radiative properties of cirrus clouds, J. Atmos. Sci., 50, 2008–2025, 1993.

Gao, K., Friebel, F., Zhou, C.-W., and Kanji, Z. A.: Enhanced soot particle ice nucleation ability induced by aggregate compaction and densification, Atmos. Chem. Phys., 22, 4985–5016, https://doi.org/10.5194/acp-22-4985-2022, 2022.

Gasparini, B., Meyer, A., Neubauer, D., Münch, S., and Lohmann, U.: Cirrus cloud properties as seen by the CALIPSO satellite and ECHA;-HAM global climate model, J. Clim. 2018, 31, 1983–2003, https://doi.org/10.1175/JCLI-D-16-0608.1, 2018.

Graf, K., Schumann, U., Mannstein, H., and Mayer, B.: Aviation induced diurnal North Atlantic cirrus cover cycle, Geophys. Res. Lett., 39, L16804, doi:10.1029/2012GL052590, 2012.

Groß, S., Tesche, M., Freudenthaler, V., Toledano, C., Wiegner, M., Ansmann, A., Althausen, D., and Seefeldner, M.: Characterization of Saharan dust, marine aerosols and mixtures of biomass-burning aerosols and dust by means of multi-wavelength depolarization and Raman lidar measurements during SAMUM 2, Tellus, 63B, 706–724, 2011.

Groß, S., Esselborn, M., Abicht, F., Wirth, M., Fix, A., Minikin, A.: Airborne high spectral resolution lidar observation of pollution aerosol during EUCAARI-LONGREX, Atmos. Chem. Phys., 13, 2435–2444, DOI: 10.5194/acp-13-2435-2013, 2013.

Groß, S., Jurkat-Witschas, T., Li, Q., Wirth, M., Urbanek, B., Krämer, M., Weigel, R., and Voigt, C.: Investigating an indirect aviation effect on mid-latitude cirrus clouds – linking lidar-derived optical properties to in situ measurements, Atmos. Chem. Phys., 23, 8369–8381, https://doi.org/10.5194/acp-23-8369-2023, 2023.

Groß, S., Freudenthaler, V., Wirth, M., Weinzierl, B.: Towards an aerosol classification scheme for future EarthCARE lidar observations and implications for research needs, Atmos. Sci. Lett., 16, 77–82, DOI: 10.1002/asl2.524, 2015.

Hersbach, H., Bell, B., Berrisford, P., Hirahara, S., Horányi, A., Muñoz-Sabater, J., Nicolas, J., Peubey, C., Radu, R., Schepers, D., Simmons, A., Soci, C., Abdalla, S., Abellan, X., Balsamo, G., Bechtold, P., Biavati, G., Bidlot, J., Bonavita, M., De Chiara, G., Dahlgren, P., Dee, D., Diamantakis, M., Dragani, R., Flemming, J., Forbes, R., Fuentes, M., Geer, A., Haimberger, L., Healy, S., Hogan, R. J., Hólm, E., Janisková, M., Keeley, S., Laloyaux, P., Lopez, P., Lupu, C., Radnoti, G., de Rosnay, P., Rozum, I., Vamborg, F., Villaume, S., and Thépaut, J. N.: The ERA5 global reanalysis, Q. J. Roy. Meteorol. Soc., 146, 1999-2049, https://doi.org/10.1002qj.3803, 2020.

https://doi.org/10.5194/egusphere-2025-2052
Preprint. Discussion started: 19 June 2025

Heymsfield, A. J., Winker, D., and van Zadelhoff, G.: Extinction-ice water content-effective radius algorithms for CALIPSO, Geophys. Res. Lett., 32, L10807, doi:10.1029/2005GL022742, 2005.

Heymsfield, A., Baumgardner, D., Demott, P., Forster, P., Gierens, K., and Kärcher, B.: Contrail microphysics, Bull. Amer. Meteor. Soc., 91, 465–472, https://doi.org/10.1175/2009BAMS2839.1, 2010.

Heymsfield, A., Winker, D., Avery, M., Vaughan, M., Diskin, G., Deng, M., Mitev, V., and Ratthey, R.: Relationships between ice water content and volume extinction coefficient from in situ observations for temperatures from 0°to –86°: Implications for spaceborne lidar retrievals, J. Appl. Meteorol. Climatol., 53, 479–505, doi:10.1175/JAMC-D-13-087.1, 2014.

Heymsfield, A. J., Krämer, M., Luebke, A., Brown, P., Cziczo, D. J., Franklin, C., Lawson, P., Lohmann, U., McFarquhar, G., Ulanowski, Z., and Van Tricht, K.: Cirrus clouds, Meteor. Mon., 58, 2.1–2.26, https://doi.org/10.1175/AMSMONOGRAPHS-D-16-0010.1, 2017.

Holland, M. M., and Bitz, C. M.: Polar amplification of climate change in coupled models. Clim. Dyn. 21, 221–232, https://doi.org/10.1007/s00382-003-0332-6, 2003.

Hoose, C. and Möhler, O.: Heterogeneous ice nucleation on atmospheric aerosols: a review of results from laboratory experiments, Atmos. Chem. Phys., 12, 9817–9854, https://doi.org/10.5194/acp-12-9817-2012, 2012.

Hong, Y. and Liu, G.: The Characteristics of Ice Cloud Properties Derived from CloudSat and CALIPSO Measurements, J. Climate, 28, 3880–3901, https://doi.org/10.1175/jcli-d-14-00666.1, 2015.

Huang J., Hitchcock P., Maycock A.C., McKenna C.M., Tian W.: Northern hemisphere cold air outbreaks are more likely to be severe during weak polar vortex conditions. Commun. Earth Environ. 2(1):147. https://doi.org/10.1038/s43247-021-00215-6, 2021.

Hunt, W. H., Winker, D. M., Vaughan, M. A., Powell, K. A., Lucker, P. L., and Weimer, C.: CALIPSO lidar description and performance assessment, J. Atmos. Oceanic Technol., 26, 1214–1228, 2009.

Hu, Y., Winker, D., Vaughan, M., Lin, B., Omar, A., Trepte, C., Flittner, D., Yang, P., Nasiri, S. L., Baum, B., Holz, R., Sun, W., Liu, Z., Wang, Z., Young, S., Stamnes, K., Huang, J., and Kuehn, R.: CALIPSO/CALIOP cloud phase discrimination algorithm, J. Atmos. Oceanic Technol., 26, 2293–2309, https://doi.org/10.1175/2009JTECHA1280.1, 2009.

Kanji, Z. A., Ladino, L. A., Wex, H., Boose, Y., BurkertKohn, M., Cziczo, D. J., and Krämer, M.: Overview of Ice Nucleating Particles, Meteor. Monogr., 58, 1–33, https://doi.org/10.1175/AMSMONOGRAPHS-D-16-0006.1, 2017.

Kärcher, B., Burkhardt, U., Bier, A., Bock, L., and Ford, I. J.: The microphysical pathway to contrail formation, J. Geophys. Res.: Atmos., 120, 7893–7927, https://doi.org/10.1002/2015JD023491, 2015.

Kärcher, B. and Lohmann, U.: A parameterization of cirrus cloud formation: Homogeneous freezing, J. Geophys. Res.-Atmos., 108, D14, 4402, https://doi.org/10.1029/2002JD003220, 2003.

Kärcher, B.: Formation and radiative forcing of contrail cirrus, Nat. Commun., 9, 1824, https://doi.org/10.1038/s41467-018-04068-0, 2018.

Kärcher, B.: Cirrus clouds and their response to anthropogenic activities, Curr. Clim. Change Rep., 3, 45–57, https://doi.org/10.1007/s40641-017-0060-3, 2017.

Kärcher, B., DeMott, P. J., Jensen, E. J., and Harrington, J. Y.: Studies on the Competition Between Homogeneous and Heterogeneous Ice Nucleation in Cirrus Formation, J. Geophys. Res.-Atmos., 127, e2021JD035805, https://doi.org/10.1029/2021JD035805, 2022.

Kienast-Sjögren, E., Rolf, C., Seifert, P., Krieger, U. K., Luo, B. P., Krämer, M., and Peter, T.: Climatological and radiative properties of midlatitude cirrus clouds derived by automatic evaluation of lidar measurements, Atmos. Chem. Phys., 16, 7605–7621, https://doi.org/10.5194/acp-16-7605-2016, 2016.

Koop, T., Luo, B., Tsias, A., and Peter, T.: Water activity as the determinant for homogeneous ice nucleation in aqueous solutions, Nature, 406, 611, https://doi.org/10.1038/35020537, 2000.

https://doi.org/10.5194/egusphere-2025-2052
Preprint. Discussion started: 19 June 2025

Kulkarni, G., China, S., Liu, S., Nandasiri, M., Sharma, N., Wilson, J., Aiken, A. C., Chand, D., Laskin, A., Mazzoleni, C., Pekour, M., Shilling, J., Shutthanandan, V., Zelenyuk, A., and Zaveri, R. A.: Ice nucleation activity of diesel soot particles at cirrus relevant temperature conditions: Effects of hydration, secondary organics coating, soot morphology, and coagulation. Geophys. Res. Lett., 43(7):3580–3588, doi:10.1002/2016GL068707, 2016.

Krämer, M., Rolf, C., Luebke, A., Afchine, A., Spelten, N., Costa, A., Meyer, J., Zöger, M., Smith, J., Herman, R. L., Buchholz, B., Ebert, V., Baumgardner, D., Borrmann, S., Klingebiel, M., Avallone, L.: A microphysics guide to cirrus clouds – Part 1: Cirrus types, Atmos. Chem. Phys., 16, 3463–3483, doi:10.5194/acp-16-3463-2016, 2016.

Krämer, M., Rolf, C., Spelten, N., Afchine, A., Fahey, D., Jensen, E., Khaykin, S., Kuhn, T., Lawson, P., Lykov, A., Pan, L. L., Riese, M., Rollins, A., Stroh, F., Thornberry, T., Wolf, V., Woods, S., Spichtinger, P., Quaas, J., and Sourdeval, O.: A microphysics guide to cirrus – Part 2: Climatologies of clouds and humidity from observations, Atmos. Chem. Phys., 20, 12569–12608, https://doi.org/10.5194/acp-20-12569-2020, 2020.

Lawrence, Z. D., Perlwitz, J., Butler, A. H., Manney, G. L., Newman, P. A., Lee, S. H., and Nash, E. R.: The remarkably strong Arctic stratospheric polar vortex of winter 2020: Links to record-breaking Arctic oscillation and ozone loss, J. Geophys. Res., 125(22), e2020JD033271. https://doi.org/10.1029/2020JD033271, 2020.

Lee, D. S., Fahey, D. W., Skowron, A., Allen, M. R., Burkhardt, U., Chen, Q., Doherty, S. J., Freeman, S., Forster, P. M., Fuglestvedt, J., Gettelman, A., De León, R. R., Lim, L. L., Lund, M. T., Millar, R. J., Owen, B., Penner, J. E., Pitari, G., Prather, M. J., Sausen, R., Wilcox, L. J.: The contribution of global aviation to anthropogenic climate forcing for 2000 to 2018, Atmos. Environ., 244, 117834, https://doi.org/10.1016/j.atmosenv.2020.117834, 2021.

Li, Q., and Groß, S.: Changes in cirrus cloud properties and occurrence over Europe during the COVID-19-caused air traffic reduction, Atmos. Chem. Phys., 21, 14573–14590, https://doi.org/10.5194/acp-21-14573-2021, 2021.

Li, Q., and Groß, S.: Satellite observations of seasonality and long-term trends in cirrus cloud properties over Europe: investigation of possible aviation impacts, Atmos. Chem. Phys., 22, 15963–15980, https://doi.org/10.5194/acp-22-15963-2022, 2022.

Liou, K. N.: Influence of cirrus clouds on weather and climate processes: A global perspective, Mon. Weather Rev., 114, 1167–1199, 1986.

Liu, Z., Vaughan, M., Winker, D., Hostetler, C., Poole, L., Hlavka, D., Hart, W., and McGill, M.: Use of probability distribution functions for discriminating between cloud and aerosol in lidar backscatter data, J. Geophys. Res., 109, D15202, doi:10.1029/2004JD004732, 2004.

Liu, Z., Vaughan, M., Winker, D., Kittaka, C., Getzewich, B., Kuehn, R., Omar, A., Powell, K., Trepte, C., and Hostetler, C.: The CALIPSO lidar cloud and aerosol discrimination: Version 2 algorithm and initial assessment of performance, J. Atmos. Oceanic Technol., 26, 1198–1213, https://doi.org/10.1175/2009JTECHA1229.1, 2009.

Lolli, S., Campbell, J.R., Lewis, J.R., Gu, Y., Marquis, J.W., Chew, B.N., Liew, S.C., Salinas, S.V., Welton, E.J.: Daytime top-of-the-atmosphere cirrus cloud radiative forcing properties at Singapore. J. Appl. Meteorol. Climatol., 56, 1249–1257, https://doi.org/10.1175/JAMC-D-16-0262.1, 2017.

Luebke, A. E., Avallone, L. M., Schiller, C., Meyer, J., Rolf, C., and Krämer, M.: Ice water content of Arctic, midlatitude, and tropical cirrus – Part 2: Extension of the database and new statistical analysis, Atmos. Chem. Phys., 13, 6447–6459, https://doi.org/10.5194/acp-13-6447-2013, 2013

Luebke, A. E., Afchine, A., Costa, A., Grooß, J.-U., Meyer, J., Rolf, C., Spelten, N., Avallone, L. M., Baumgardner, D., and Krämer, M.: The origin of midlatitude ice clouds and the resulting influence on their microphysical properties, Atmos. Chem. Phys., 16, 5793–5809, https://doi.org/10.5194/acp-16-5793-2016, 2016.

https://doi.org/10.5194/egusphere-2025-2052
Preprint. Discussion started: 19 June 2025

Marquis, J. W., Dolinar, E. K., Garnier, A., Campbell, J. R. Ruston, B. C., Yang, P., and Zhang, J.: Estimating the impact of assimilating cirrus cloud - contaminated hyperspectral infrared radiances for numerical weather prediction, J. Atmos. Oceanic Technol, 40, 327–340, https://doi.org/10.1175/JTECH-D-21-0165.1, 2023.

Mahrt, F., Marcolli, C., David, R. O., Grönquist, P., Barthazy Meier, E. J., Lohmann, U., and Kanji, Z. A.: Ice nucleation abilities of soot particles determined with the Horizontal Ice Nucleation Chamber, Atmos. Chem. Phys., 18, 13363–13392, https://doi.org/10.5194/acp-18-13363-2018, 2018.

Manney, G. L., Millán, L. F., Santee, M. L., Wargan, K., Lambert, A., Neu, J. L., Werner, F., Lawrence, Z. D., Schwartz, M. J., Livesey, N. J., and Read, W. G., Signatures of anomalous transport in the 2019/2020 Arctic stratospheric polar vortex. J. Geophys. Res.: Atmospheres, 127(20). https://doi.org/10.1029/2022jd037407, 2022.

Marsing, A., Meerkötter, R., Heller, R., Kaufmann, S., JurkatWitschas, T., Krämer, M., Rolf, C., and Voigt, C.: Investigating the radiative effect of Arctic cirrus measured in situ during the winter 2015–2016, Atmos. Chem. Phys., 23, 587–609, https://doi.org/10.5194/acp-23-587-2023, 2023.

Martin, C., and Platt, R.: A Parameterization of the Visible Extinction Coefficient of Ice Clouds in Terms of the Ice/Water Content, J. Atmos. Sci., 54(16), 2083–2098, https://doi.org/10.1175/1520-0469(1997)054<2083:APOTVE>2.0.CO;2, 1997.

McCrystall, M.R., Stroeve, J., Serreze, M., Forbes, B. C., and Screen, J. A.: New climate models reveal faster and larger increases in Arctic precipitation than previously projected. Nat Commun 12, 6765, https://doi.org/10.1038/s41467-021-27031-y, 2021.

Mewes, D. and Jacobi, C.: Heat transport pathways into the Arctic and their connections to surface air temperatures, Atmos. Chem. Phys., 19, 3927–3937, https://doi.org/10.5194/acp-19-3927-2019, 2019.

Mioche, G., Josset, D., Gayet, J.-F., Pelon, J., Garnier, A., Minikin, A., and Schwarzenboeck, A.: Validation of the CALIPSO-CALIOP extinction coefficients from in situ observations in midlatitude cirrus clouds during the CIRCLE-2 experiment, J. Geophys. Res., 115, D00H25, doi:10.1029/2009JD012376, 2010.

Murphy, D. M., Froyd, K. D., Bian, H., Brock, C. A., Dibb, J. E., DiGangi, J. P., Diskin, G., Dollner, M., Kupc, A., Scheuer, E. M., Schill, G. P., Weinzierl, B., Williamson, C. J., and Yu, P.: The distribution of sea-salt aerosol in the global troposphere, Atmos. Chem. Phys., 19, 4093–4104, https://doi.org/10.5194/acp-19-4093-2019, 2019.

NASA: CALIPSO Data User's Guide – Data Product Description – Lidar Level 2 Vertical Feature Mask (VFM) Version 4.x Product, available at: https://asdc.larc.nasa.gov/project/CALIPSO/CAL_LID_L2_VFM-Standard-V4-20_V4-20/, last access: 13 March 2025, 2025a.

NASA: CALIPSO Search and Subsetting web application, NASA Langley Research Center Atmospheric Science Data Center, available at: https://subset.larc.nasa.gov/calipso/login.php, last access: 13 March 2025, 2025b.

Nazaryan, H., McCormick, M. P., and Menzel, W. P.: Global characterization of cirrus clouds using CALIPSO data, J. Geophys. Res., 113, D16211, doi:10.1029/2007JD009481, 2008.

Omar, A. H., Winker, D. M., Vaughan, M. A., Hu, Y., Trepte, C. R., Ferrare, R. A., Lee, K.-P., Hostetler, C. A., Kittaka, C., Rogers, R. R., Kuehn, R. E., and Liu, Z.: The CALIPSO automated aerosol classification and lidar ratio selection algorithm, J. Atmos. Oceanic Technol., 26, 1994–2014, https://doi.org/10.1175/2009JTECHA1231.1, 2009.

Pithan, F., Svensson, G., Caballero, R., Chechin, D., Cronin, T. W., Ekman, A. M. L., Neggers, R., Shupe, M. D., Solomon, A., Tjernström, M., and Wendisch, M.: Role of air-mass transformations in exchange between the Arctic and mid-latitudes, Nat. Geosci., 11, 805–812, https://doi.org/10.1038/s41561-018-0234-1, 2018.

https://doi.org/10.5194/egusphere-2025-2052
Preprint. Discussion started: 19 June 2025

Platt, C. M. R., Young, S. A., Manson, P. J., Patterson, G. R., Marsden, S. C., Austin, R. T., and Churnside, J. H.: The optical properties of equatorial cirrus from observations in the ARM pilot radiation observation experiment, J. Atmos. Sci., 55, 1977–1996, https://doi.org/10.1175/1520-0469(1998)055<1977:TOPOEC>2.0.CO;2, 1998.

Platt, C. M. R., Young, S. A., Austin, R. T., Patterson, G. R., Mitchell, D. L., and Miller, S. D.: LIRAD Observations of Tropical Cirrus Clouds in MCTEX. Part I: Optical Properties and Detection of Small Particles in Cold Cirrus, J. Atmos. Sci., 59, 3145–3162, https://doi.org/10.1175/1520-0469(2002)059<3145:LOOTCC>2.0.CO;2, 2002.

Quaas, J., E. Gryspeerdt, R. Vautard, and O. Boucher, Climate impact of aircraft-induced cirrus assessed from satellite observations before and during COVID-19, *Environ. Res. Lett.*, *16*, 064051, doi:10.1088/1748-9326/abf686, 2021.

Quaas, J., Andrews, T., Bellouin, N., Block, K., Boucher, O., Ceppi, P., Dagan, G., Doktorowski, S., Eichholz, H., Forster, P., Goren, T., Gryspeerdt, E., Hodnebrog, O., Jia, H., Kramer, R., Lange, C., Maycock, A., Mülmenstädt, J., Myhre, G., O'Connor, F., Pincus, R., Samset, B., Senf, F., Shine, K., Smith, C., Stjern, C., Takemura, T., Toll, V., and Wall, C.: Adjustments to climate perturbations - mechanisms, implications, observational constraints, AGU Advances, 5, e2023AV001144, doi:10.1029/2023AV001144, 2024.

Ratcliffe, N. G., Ryder, C. L., Bellouin, N., Woodward, S., Jones, A., Johnson, B., Wieland, L.-M., Dollner, M., Gasteiger, J., and Weinzierl, B.: Long-range transport of coarse mineral dust: an evaluation of the Met Office Unified Model against aircraft observations, Atmos. Chem. Phys., 24, 12161–12181, https://doi.org/10.5194/acp-24-12161-2024, 2024.

Rantanen, M., Karpechko, A., Lipponen, A., Nordling, K., Hyvärinen, O., Ruosteenoja, K., Vihma, T., and Laaksonen, A.: The Arctic has warmed nearly four times faster than the globe since 1979, Commun. Earth Environ., 3, 168, https://doi.org/10.1038/s43247-022-00498-3, 2022.

Rogers, D. C., DeMott, P. J., Kreidenweis, S. M., and Chen, Y.: Measurements of ice nucleating aerosols during SUCCESS, Geophys. Res. Lett., 25, 1383–1386, https://doi.org/10.1029/97gl03478, 1998.

Rosinski, J., and Morgan, G.M.: Ice-forming nuclei in transvaal, Republic of South Africa. J. Aerosol Sci., 19, 531–538, 1988.

Righi, M., Hendricks, J., and Beer, C. G.: Exploring the uncertainties in the aviation soot–cirrus effect, Atmos. Chem. Phys., 21, 17267–17289, https://doi.org/10.5194/acp-21-17267-2021, 2021.

Sassen, K. and Campbell, J. R.: A midlatitude cirrus cloud climatology from the facility for atmospheric remote sensing. Part I: Macrophysical and synoptic properties, J. Atmos. Sci., 58, 481–496, https://doi.org/10.1175/1520-0469(2001)058<0481:AMCCCF>2.0.CO;2, 2001.

Sassen, K. and Benson, S.: A midlatitude cirrus cloud climatology from the facility for atmospheric remote sensing. Part II: Microphysical properties derived from lidar depolarization, J. Atmos. Sci., 58, 2103–2112, https://doi.org/10.1175/1520-0469(2001)058<2103:AMCCCF>2.0.CO;2, 2001.

Sassen, K., Wang, Z., and Liu, D.: Global distribution of cirrus clouds from CloudSat/Cloud-Aerosol Lidar and Infrared Pathfinder Satellite Observations (CALIPSO) measurements, J. Geophys. Res., 113, D00A12, doi:10.1029/2008JD009972, 2008.

Sassen, K. and Zhu, J.: A global survey of CALIPSO linear depolarization ratios in ice clouds: Initial findings, J. Geophys. Res., 114, D00H07, https://doi.org/10.1029/2009JD012279, 2009.

Sato, K., Takahashi, k., and Inoue, J.: Impact of Canadian wildfires on aerosol and ice clouds in the early-autumn Arctic. Atmos. Res., 315: 107893 DOI: 10.1016/j.atmosres.2024.107893, 2025.

Schiller, C., Krämer, M., Afchine, A., Spelten, N., and Sitnikov, N.: Ice water content of Arctic, midlatitude, and tropical cirrus, J. Geophys. Res.-Atmos., 113, D24208, https://doi.org/10.1029/2008JD010342, 2008.

Schumann, U. and Graf, K.: Aviation-induced cirrus and radiation changes at diurnal timescales, J. Geophys. Res., 118, 2404–2421, doi:10.1002/jgrd.50184, 2013.

https://doi.org/10.5194/egusphere-2025-2052
Preprint. Discussion started: 19 June 2025

Schumann, U., Poll, I., Teoh, R., Koelle, R., Spinielli, E., Molloy, J., Koudis, G. S., Baumann, R., Bugliaro, L., Stettler, M., and Voigt, C.: Air traffic and contrail changes during COVID-19 over Europe: A model study, Atmos. Chem. Phys., 21, 7429–7450, https://doi.org/10.5194/acp-21-7429-2021, 2021.

Schumann, U., Bugliaro, L., Dörnbrack, A., Baumann, R., and Voigt, C.: Aviation contrail cirrus and radiative forcing over Europe during 6 months of COVID-19, Geophys. Res. Lett., 48, e2021GL092771, https://doi.org/10.1029/2021GL092771, 2021.

Serreze, M. C. and Barry, R. G.: Processes and impacts of Arctic amplification: A research synthesis, Global Planet. Change, 77, 85–96, https://doi.org/10.1016/j.gloplacha.2011.03.004, 2011.

Serreze, M. C., Barrett, A. P., Stroeve, J. C., Kindig, D. N., and Holland, M. M.: The emergence of surface-based Arctic amplification, The Cryosphere, 3, 11–19, https://doi.org/10.5194/tc-3-11-2009, 2009.

Stephens, G. L., Wood, N. B., Gabriel, P. M.: An assessment of the parameteirzation of subgrid-scale cloud effects on radiative transfer. Part I: Vertical overlap, J. Atmos. Sci. 61, 715–732. doi: 10.1175/1520-0469(2004)061<0715:aaotpo>2.0.co;2, 2004.

Stephens, G., Winker, D. M., Pelon, J., Trepte, C., Vane, D., Yuhas, C., L'Ecuyer, T., and Lebsock, M.: CloudSat and CALIPSO within the A-Train: Ten years of actively observing the Earth system, Bull. Amer. Meteor. Soc., 99, 569–581, https://doi.org/10.1175/BAMS-D-16-0324.1, 2018.

Stettler, M. E., Boies, A. M., Petzold, A., and Barrett, S. R.: Global civil aviation black carbon emissions, Environ. Sci. Technol., 47, 10397–10404, https://doi.org/10.1021/es401356v, 2013.

Tang, M. J., Cziczo, D. J., and Grassian, V. H. (2016). Interactions of water with mineral dust aerosol: Water adsorption, hygroscopicity, cloud condensation, and ice nucleation. Chemical Reviews, 116(7), 4205–4259. https://doi.org/10.1021/acs.chemrev.5b00529, 2016.

Takano, Y. and Liou, K. N.: Solar radiative transfer in cirrus clouds. Part I: Single-scattering and optical properties of hexagonal ice crystals, J. Atmos. Sci., 46, 3–19, https://doi.org/10.1175/1520-0469(1989)046<0003:SRTICC>2.0.CO;2, 1989.

Tesche, M., Ansmann, A., Müller, D., Althausen, D., Engelmann, R., Freudenthaler, V., and Groß, S.: Vertically resolved separation of dust and smoke over Cape Verde using multi-wavelength Raman and polarization lidars during Saharan Mineral Dust Experiment 2008, J. Geophys. Res., 114, D13202, doi:10.1029/2009JD011862, 2009.

Tesche, M., Achtert, P., Glantz, P., and Noone, K. J.: Aviation effects on already-existing cirrus clouds, Nat. Commun., 7(1), 12016, https://doi.org/10.1038/ncomms12016, 2016.

Teoh, R., Engberg, Z., Shapiro, M., Dray, L., and Stettler, M. E. J.: The high-resolution Global Aviation emissions Inventory based on ADS-B (GAIA) for 2019–2021, Atmos. Chem. Phys., 24, 725–744, https://doi.org/10.5194/acp-24-725-2024, 2024.

Testa, B., Durdina, L., Alpert, P. A., Mahrt, F., Dreimol, C. H., Edebeli, J., Spirig, C., Decker, Z. C. J., Anet, J., and Kanji, Z. A.: Soot aerosols from commercial aviation engines are poor ice-nucleating particles at cirrus cloud temperatures, Atmos. Chem. Phys., 24, 4537–4567, https://doi.org/10.5194/acp-24-4537-2024, 2024.

Testa, B., Durdina, L., Edebeli, J., Spirig, C., and Kanji, Z. A.: Simulated contrail-processed aviation soot aerosols are poor ice-nucleating particles at cirrus temperatures, Atmos. Chem. Phys., 24, 10409–10424, https://doi.org/10.5194/acp-24-10409-2024, 2024.

Urbanek, B., Groß, S., Wirth, M., Rolf, C., Krämer, M., and Voigt, C.: High depolarization ratios of naturally occurring cirrus clouds near air traffic regions over Europe, Geophys. Res. Lett., 45, 13,166–13,172, https://doi.org/10.1029/2018GL079345, 2018.

Vaughan, M., Young, S., Winker, D., Powell, K., Omar, A., Liu, Hu., Y., and Hostetler, C.: Fully automated analysis of space-based lidar data: An overview of the CALIPSO retrieval algorithms and data products, Proc. SPIE, 5575, 1177–1180, 2004.

https://doi.org/10.5194/egusphere-2025-2052
Preprint. Discussion started: 19 June 2025

Vaughan, M. A., Powell, K. A., Kuehn, R. E., Young, S. A., Winker, D. M., Hostetler, C. A., Hunt, W. H., Liu, Z., McJill, M. J., and Getzewich, B. J.: Fully automated detection of cloud and aerosol layers in the CALIPSO lidar measurements, j. Atmos. Oceanic Technol., 26, 2034–2050, https://doi.org/10.1175/2009JTECHA1228.1, 2009.

Voigt, C., Schumann, U., Jessberger, P., Jurkat, T., Petzold, A., Gayet, J.-F., Krämer, M., Thornberry, T., and Fahey, D. W.: Extinction and optical depth of contrails, Geophys. Res. Lett., 38, L11806, doi:10.1029/2011GL047189, 2011.

Wehr, T., Kubota, T., Tzeremes, G., Wallace, K., Nakatsuka, H., Ohno, Y., Koopman, R., Rusli, S., Kikuchi, M., Eisinger, M., Tanaka, T., Taga, M., Deghaye, P., Tomita, E., and Bernaerts, D.: The EarthCARE mission – science and system overview, Atmos. Meas. Tech., 16, 3581–3608, https://doi.org/10.5194/amt-16-3581-2023, 2023.

Wendisch, M., Macke, A., Ehrlich, A., Lüpkes, C., Mech, M., Chechin, D., Dethloff, K., Velasco, C. B., Bozem, H., Brückner, M., Clemen, H.-C., Crewell, S., Donth, T., Dupuy, R., Ebell, K., Egerer, U., Engelmann, R., Engler, C., Eppers, O., Gehrmann, M., Gong, X., Gottschalk, M., Gourbeyre, C., Griesche, H., Hartmann, J., Hartmann, M., Heinold, B., Herber, A., Herrmann, H., Heygster, G., Hoor, P.,Jafariserajehlou, S., Jäkel, E., Järvinen, E., Jourdan, O., Kästner, U., Kecorius, S., Knudsen, E. M., Köllner, F., Kretzschmar, J., Lelli, L., Leroy, D., Maturilli, M., Mei, L., Mertes, S., Mioche, G., Neuber, R., Nicolaus, M., Nomokonova, T., Notholt, J., Palm, M., van Pinxteren, M., Quaas, J., Richter, P., Ruiz-Donoso, E., Schäfer, M., Schmieder, K., Schnaiter, M., Schneider, J., Schwarzenböck, A., Seifert, P., Shupe, M. D., Siebert, H., Spreen, G., Stapf, J., Stratmann, F., Vogl, T., Welti, A., Wex, H., Wiedensohler, A., Zanatta, M., and Zeppenfeld, S.: The Arctic Cloud Puzzle: Using ACLOUD/PASCAL Multiplatform Observations to Unravel the Role of Clouds and Aerosol Particles in Arctic Amplification, Bull. Am. Meteorol. Soc., 100, 841–871, https://doi.org/10.1175/BAMS-D-18-0072.1, 2019.

Wendisch, M., Brückner, M., Crewell, S., Ehrlich, A., Notholt, J., Lüpkes, C., Macke, A., Burrows, J. P., Rinke, A., Quaas, J., Maturilli, M., Schemann, V., Shupe, M. D., Akansu, E. F., Barrientos-Velasco, C., Bärfuss, K., Blechschmidt, A.-M., Block, K., Bougoudis, I., Bozem, H., Böckmann, C., Bracher, A., Bresson, H., Bretschneider, L., Buschmann, M., Chechin, D. G., Chylik, J., Dahlke, S., Deneke, H., Dethloff, K., Donth, T., Dorn, W., Dupuy, R., Ebell, K., Egerer, U., Engelmann, R., Eppers, O., Gerdes, R., Gierens, R., Gorodetskaya, I. V., Gottschalk, M., Griesche, H., Gryanik, V. M., Handorf, D., Harm-Altstädter, B., Hartmann, J., Hartmann, M., Heinold, B., Herber, A., Herrmann, H., Heygster, G., Höschel, I., Hofmann, Z., Hölemann, J., Hünerbein, A., Jafariserajehlou, S., Jäkel, E., Jacobi, C., Janout, M., Jansen, F., Jourdan, O., Jurányi, Z., Kalesse-Los, H., Kanzow, T., Käthner, R., Kliesch, L. L., Klingebiel, M., Knudsen, E. M., Kovács, T., Körtke, W., Krampe, D., Kretzschmar, J., Kreyling, D., Kulla, B., Kunkel, D., Lampert, A., Lauer, M., Lelli, L., von Lerber, A., Linke, O., Löhnert, U., Lonardi, M., Losa, S. N., Losch, M., Maahn, M., Mech, M., Mei, L., Mertes, S., Metzner, E., Mewes, D., Michaelis, J., Mioche, G., Moser, M., Nakoudi, K., Neggers, R., Neuber, R., Nomokonova, T., Oelker, J., Papakonstantinou-Presvelou, I., Pätzold, F., Pefanis, V., Pohl, C., van Pinxteren, M., Radovan, A., Rhein, M., Rex, M., Richter, A., Risse, N., Ritter, C., Rostosky, P., Rozanov, V. V., Donoso, E. R., Saavedra Garfias, P., Salzmann, M., Schacht, J., Schäfer, M., Schneider, J., Schnierstein, N., Seifert, P., Seo, S., Siebert, H., Soppa, M. A., Spreen, G., Stachlewska, I. S., Stapf, J., Stratmann, F., Tegen, I., Viceto, C., Voigt, C., Vountas, M., Walbröl, A., Walter, M., Wehner, B., Wex, H., Willmes, S., Zanatta, M., and Zeppenfeld, S.: Atmospheric and Surface Processes, and Feedback 925 Mechanisms Determining Arctic Amplification: A Review of First Results and Prospects of the (AC)3 Project, Bull. Am. Meteorol. Soc., 104, E208–E242, https://doi.org/10.1175/BAMS-D-21-0218.1, 2023.

Voigt, C., Schumann, U., Minikin, A., Abdelmonem, A., Afchine, A., Borrmann, S., Boettcher, M., Buchholz, B., Bugliaro, L., Costa, A., Curtius, J., Dollner, M., Dörnbrack, A., Dreiling, V., Ebert, V., Ehrlich, A., Fix, A., Forster, L., Frank, F., Fütterer, D., Giez, A., Graf, K., Grooß, J.-U., Groß, S., Heimerl, K., Heinold, B., Hüneke, T., Järvinen, E., Jurkat, T., Kaufmann, S., Kenntner, M., Klingebiel, M., Klimach, T., Kohl, R., Krämer, M., Krisna, T. C., Luebke, A., Mayer, B., Mertes, S., Molleker, S., Petzold, A., Pfeilsticker, K., Port, M., Rapp, M., Reutter, P., Rolf, C., Rose, D., Sauer, D., Schäfler, A., Schlage, R., Schnaiter, M., Schneider, J., Spelten, N., Spichtinger, P.,

https://doi.org/10.5194/egusphere-2025-2052
Preprint. Discussion started: 19 June 2025

Stock, P., Walser, A., Weigel, R., Weinzierl, B., Wendisch, M., Werner, F., Wernli, H., Wirth, M., Zahn, A., Ziereis, H., and Zöger, M.: ML-CIRRUS: The airborne experiment on natural cirrus and contrail cirrus with the high-altitude long-range research aircraft HALO, Bull. Amer. Meteor. Soc., 98, 271–288, https://doi.org/10.1175/BAMS-D-15-00213.1, 2017.

Voigt, C., Lelieveld, J., Schlager, H., Schneider, J., Curtius, J., Meerkötter, R., Sauer, D., Bugliaro, Luca., Bohn, B., Crowley, J. N., Erbertseder, T., Groß, S., Hahn, V., Li, Q., Mertens, M., Pöhlker, M. L., Pozzer, A., Schumann, U., Tomsche, L., Williams, J., Zahn, A., Andreae, M., Borrmann, S., Bräuer, T., Dörich, R., Dörnbrack, A., Edtbauer, A., Ernle, L., Fischer, H., Giez, A., Granzin, M., Grewe, V., Harder, H., Heinritzi, M., Holanda, B. A., Jöckel, P., Kaider, K., Krüger, O. O., Lucke, J., Marsing, A., Martin, A., Matthes, S., Pöhlker, C., Pöschl, U., Reifenberg, S., Ringsdorf, A., Scheibe, M., Tadic, I., Zauner-Wieczorek, M., Henke, R., Rapp, M.: Cleaner skies during the COVID-19 lockdown, Bull. Amer. Meteor. Soc., https://doi.org/10.1175/BAMS-D-21-0012.1, 2022.

Wagner, R., Ickes, L., Bertram, A. K., Els, N., Gorokhova, E., Möhler, O., Murray, B. J., Umo, N. S., and Salter, M. E.: Heterogeneous ice nucleation ability of aerosol particles generated from Arctic sea surface microlayer and surface seawater samples at cirrus temperatures, Atmos. Chem. Phys., 21, 13903–13930, https://doi.org/10.5194/acp-21-13903-2021, 2021.

Wang, P., Minnis, P., McCormick, M. P., Kent, G. S., and Skeens, K. M.: A 6-year climatology of cloud occurrence frequency from SAGE II observations (1985–1990), J. Geophys. Res., 101, 407–429, 1996.

Winker, D. M., Vaughan, M. A., Omar, A., Hu, Y., and Powell, K. A.: Overview of the CALIPSO mission and CALIOP data processing algorithms, J. Atmos. Oceanic Technol., 26, 2310–2323, https://doi.org/10.1175/2009JTECHA1281.1, 2009.

Winker, D. M., Pelon, J., Coakley Jr., J. A., Ackerman, S. A., Charlson, R. J., Colarco, P. R., Flamant, P., Fu, Q., Hoff, R. M., Kittaka, C., Kubar, T. L., Le Treut, H., Mccormick, M. P., Mégie, G., Poole, L., Powell, K., Trepte, C., Vaughan, M. A., and Wielicki, B. A.: The CALIPSO Mission: A global 3D view of aerosols and clouds, Bull. Amer. Meteor. Soc., 91, 1211–1229, https://doi.org/10.1175/2010BAMS3009.1, 2010.

Winker, D. M., Hunt, B. H., and McGill, M. J.: Initial performance assessment of CALIOP, Geophys. Res. Lett., 34, L19803, doi:10.1029/2007GL030135, 2007.

Woods, C. and Caballero, R.: The Role of Moist Intrusions in Winter Arctic Warming and Sea Ice Decline, J. Climate, 29, 4473–4485, https://doi.org/10.1175/JCLI-D-15-0773.1, 2016.

Wylie, D. P., and Menzel, W. P.: Eight years of high cloud statistics using HIRS, J. Clim., 12, 170–184, 1999.

Yu F., Kärcher B., Anderson B.E.: Revisiting Contrail Ice Formation: Impact of Primary Soot Particle Sizes and Contribution of Volatile Particles, Environ Sci Technol. 2024 Oct 8;58(40):17650-17660. doi: 10.1021/acs.est.4c04340, 2024.

Zerefos, C. S., Eleftheratos, K., Balis, D. S., Zanis, P., Tselioudis, G., and Meleti, C.: Evidence of impact of aviation on cirrus cloud formation, Atmos. Chem. Phys., 3, 1633–1644, 2003.

Zhang, Y., Macke, A, and Albers, F.: Effects of crystal size spectrum and crystal shape on stratiform cirrus radiative forcing, Atmos. Res., 52, 59–75, 1999.

https://doi.org/10.5194/egusphere-2025-2052
Preprint. Discussion started: 19 June 2025

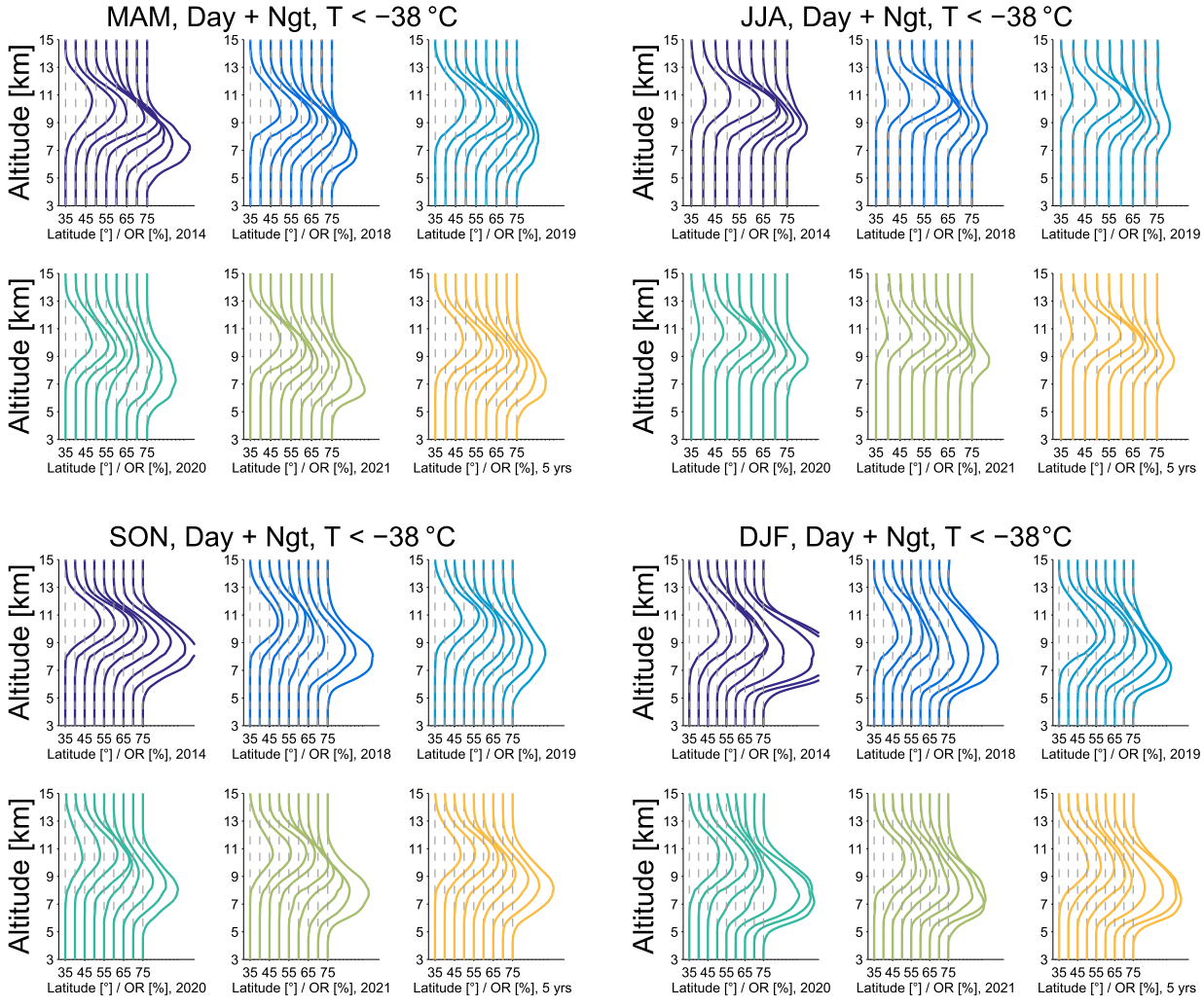

Figure 1. Profiles of occurrence rates (ORs) of cirrus clouds derived from the lidar measurements of CALIPSO in each 5-degree latitude bin from 35–80°N in different years (2014, 2018–2021) and the composite mean values from the 5-year observations. The vertical dashed lines indicating the zero levels of ORs for each bin are shifted by 3% for a better illustration. The ORs are shown in different seasons (MAM: Mar–May; JJA: Jun–Aug; SON: Sep–Nov; DJF: Dec–Feb). We note that the results of the DJF in 2014 (2018) are derived from the observations only in Jan and Feb 2014 (2018), and the rest DJF from Jan and Feb in the corresponding year and Dec from the previous year.

https://doi.org/10.5194/egusphere-2025-2052
Preprint. Discussion started: 19 June 2025

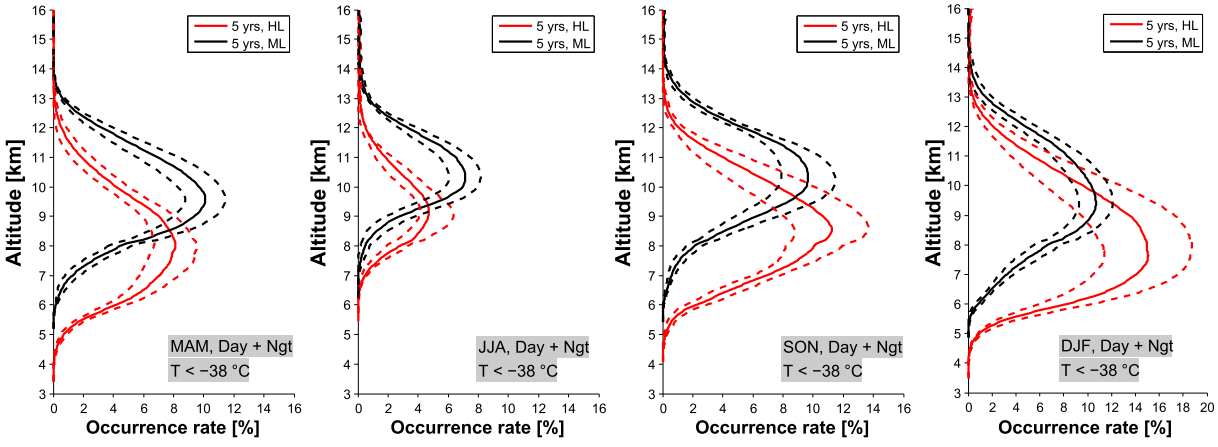

Figure 2. Profiles of occurrence rates (ORs) of cirrus clouds calculated from the composite 5-year lidar measurements of CALIPSO in different seasons at high-latitudes (60–80°N; 30°W–30°E) and midlatitudes (35–60°N; 30°W–30°E), respectively. The mean values of ORs are shown in solid lines and the standard deviations in dashed lines. The results at high- and midlatitudes are shown in red and black, respectively. Please note the different scales of x-axis for the winter results in the right-most panel.

https://doi.org/10.5194/egusphere-2025-2052
Preprint. Discussion started: 19 June 2025

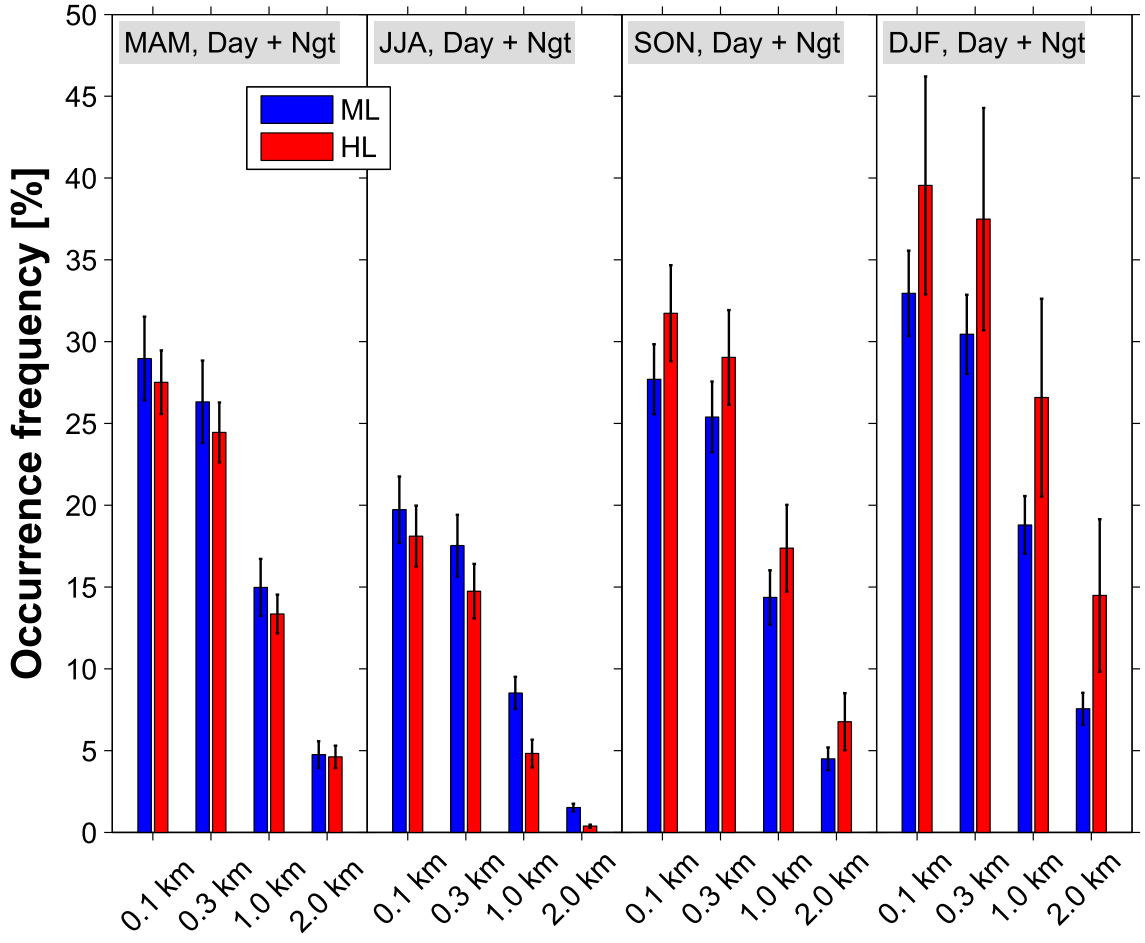

Figure 3. Occurrence frequency of the geometrical thicknesses according to the definitions with cloud thicknesses larger than 0.1, 0.3, 1.0, and 2.0 km, respectively. The composite mean values are determined in different seasons (see the caption of Figure 2 for details) at high- and midlatitudes which cover the areas of latitudes from 35–60°N and from 60–80°N, respectively, with all the lidar measurements in years of 2014 and 2018–2021. The results in spring, summer, autumn, and winter are shown in the panels from left to right. The results derived from HL and ML are shown in red and blue, respectively, along with the corresponding errorbars.

https://doi.org/10.5194/egusphere-2025-2052
Preprint. Discussion started: 19 June 2025

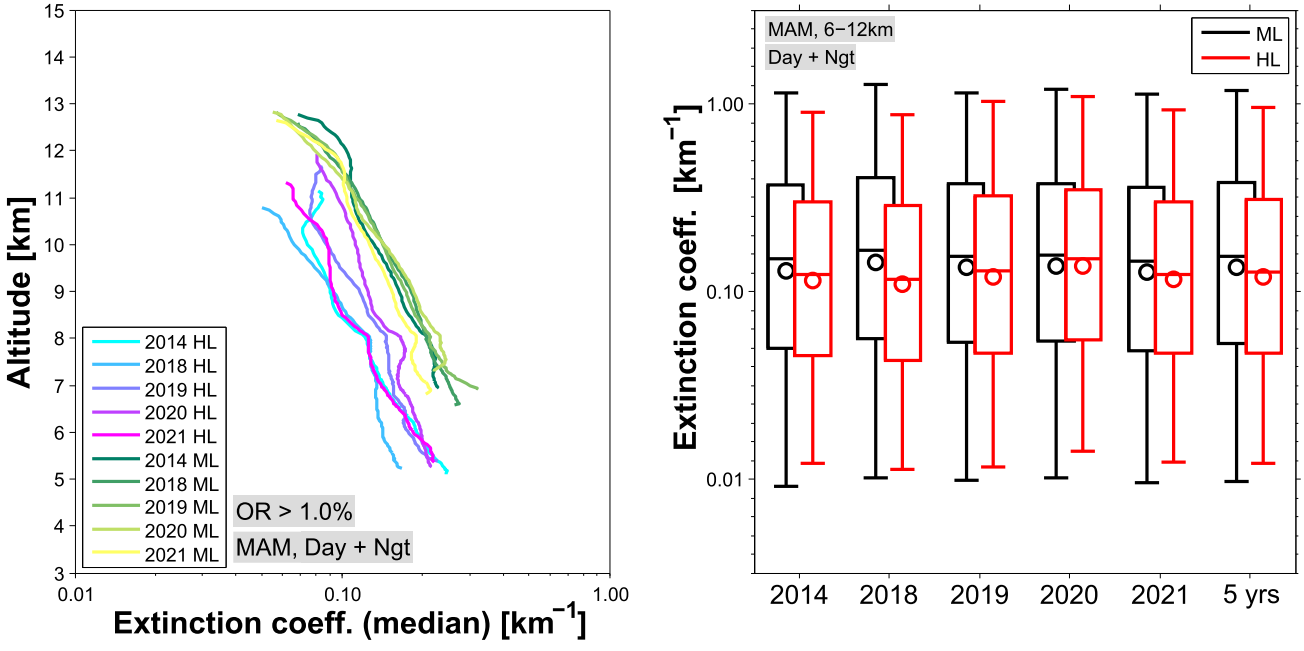

Figure 4. Left panel: Profiles of the extinction coefficient medians of ice crystals within cirrus clouds observed with CALIPSO in spring (March–May) in years of 2014 and 2018–2021. Data with the cirrus occurrence rates less than 1.0% are ignored; Right panel: Box plot representations of the extinction coefficient distributions in different year and the composite values of all the 5 years. The results in the high-latitude regions are shown in red and in the midlatitude regions in black. Boxes represent the 25th–75th percentiles of the dataset (top and bottom). Solid lines through the corresponding boxes stand for the medians and circles for the means. Whiskers indicate the 5th and 95th percentiles.

https://doi.org/10.5194/egusphere-2025-2052
Preprint. Discussion started: 19 June 2025

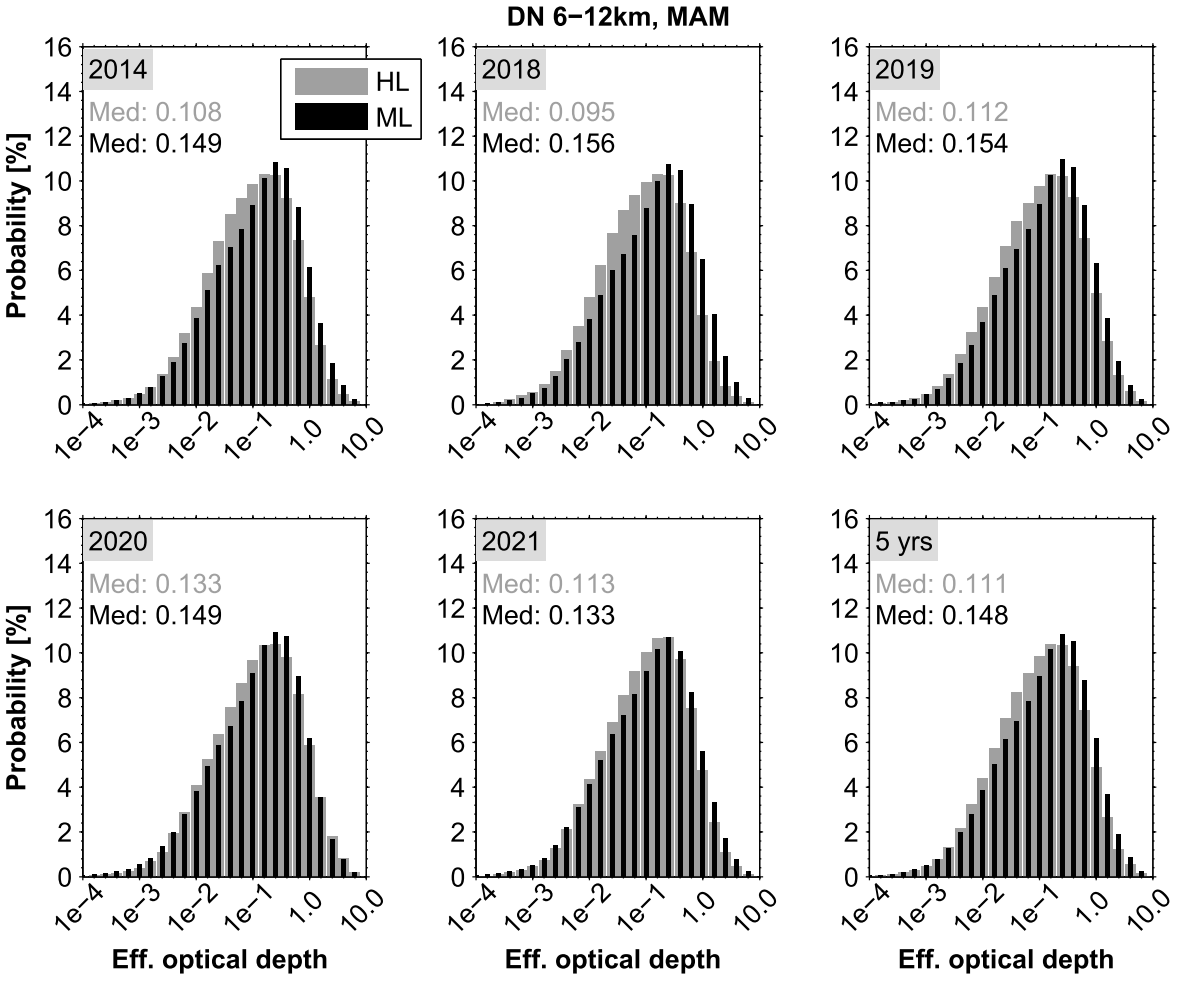

Figure 5. Histograms of effective optical depth of cirrus clouds observed in spring (March–May) in years 2014 and 2018–2021 in the high-latitude (gray) and midlatitude (black) regions, respectively. The corresponding medians for each case are indicated in the insert.

https://doi.org/10.5194/egusphere-2025-2052
Preprint. Discussion started: 19 June 2025

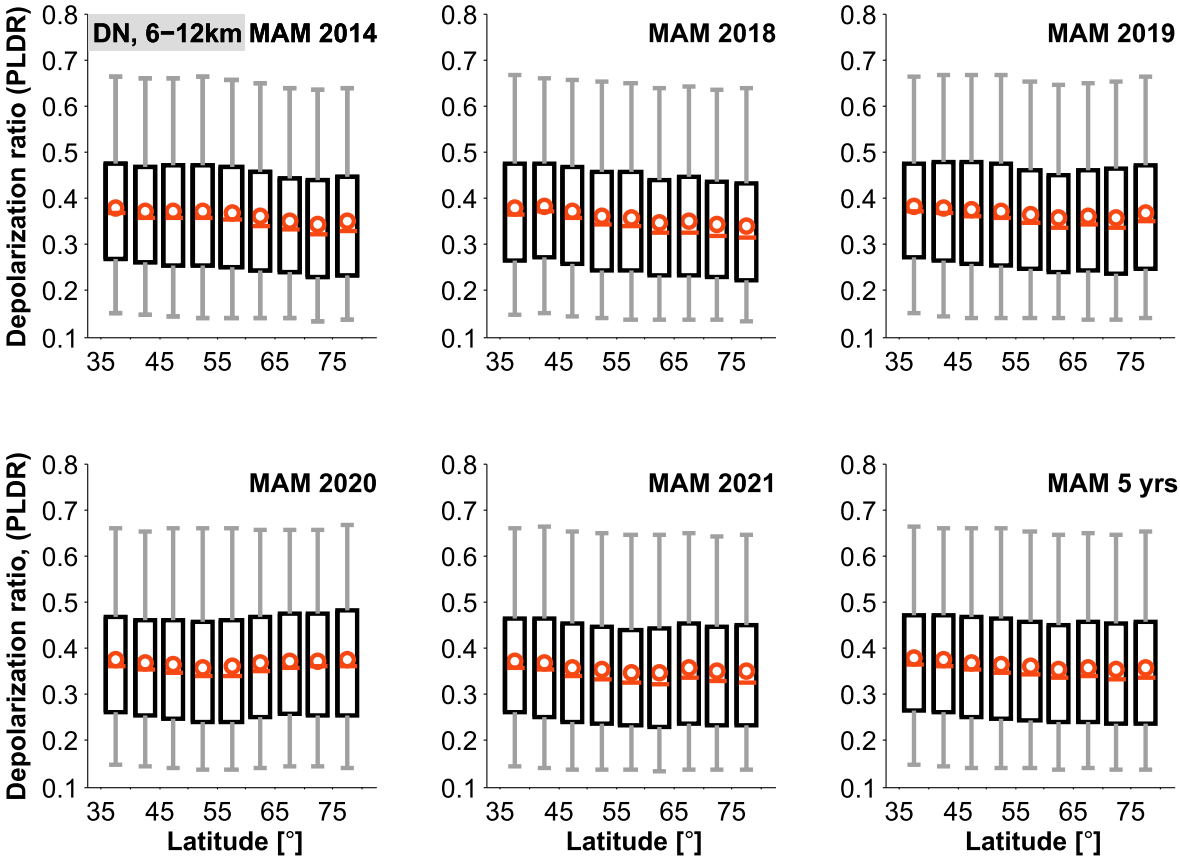

Figure 6. Box plot representations of particle linear depolarization ratios (PLDR) of cirrus clouds in each 5-degree latitude bin from 35–80°N in spring in the years 2014 and 2018–2021 as well as the composite results from all the 5 years. The descriptions of the box plot can be found in the caption of Figure 4.

https://doi.org/10.5194/egusphere-2025-2052
Preprint. Discussion started: 19 June 2025

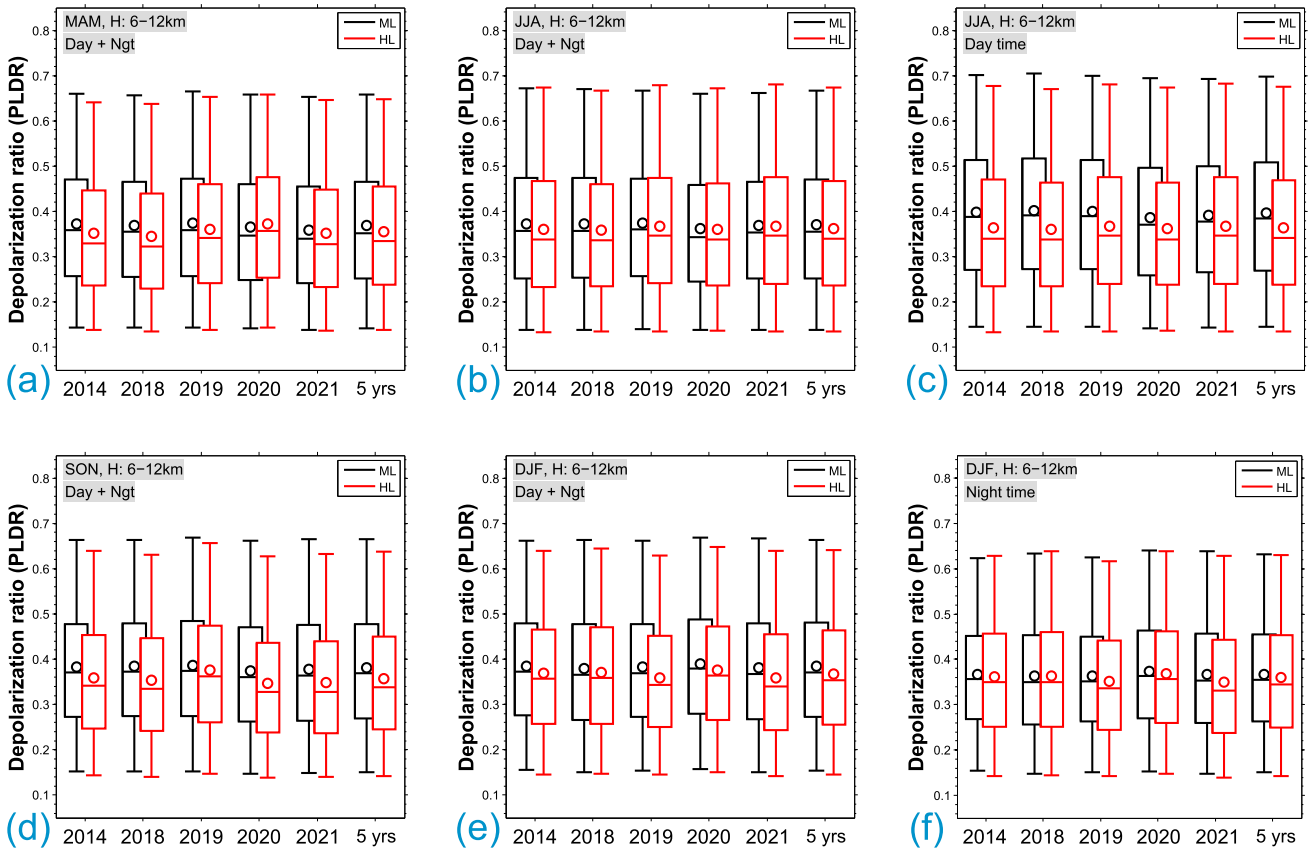

Figure 7. Box plot representations of particle linear depolarization ratios (PLDR) of cirrus clouds in different seasons in the years 2014 and 2018–2021 as well as the composite results from all the 5 years (in panels a, b, e, and f). The results in the high- and midlatitude regions are shown in red and black, respectively. Boxes represent the 25th–75th percentiles (i.e. from bottom to top of the boxes). The descriptions of the box plot can be found in the caption of Figure 4. Considering the influence of polar day and night in summer and winter, respectively, on cirrus cloud properties, we also indicate the results from only the daytime measurements in the summer months and from only the night-time measurements in winter for a fair comparison in different latitudes (in panels c and f).

https://doi.org/10.5194/egusphere-2025-2052
Preprint. Discussion started: 19 June 2025

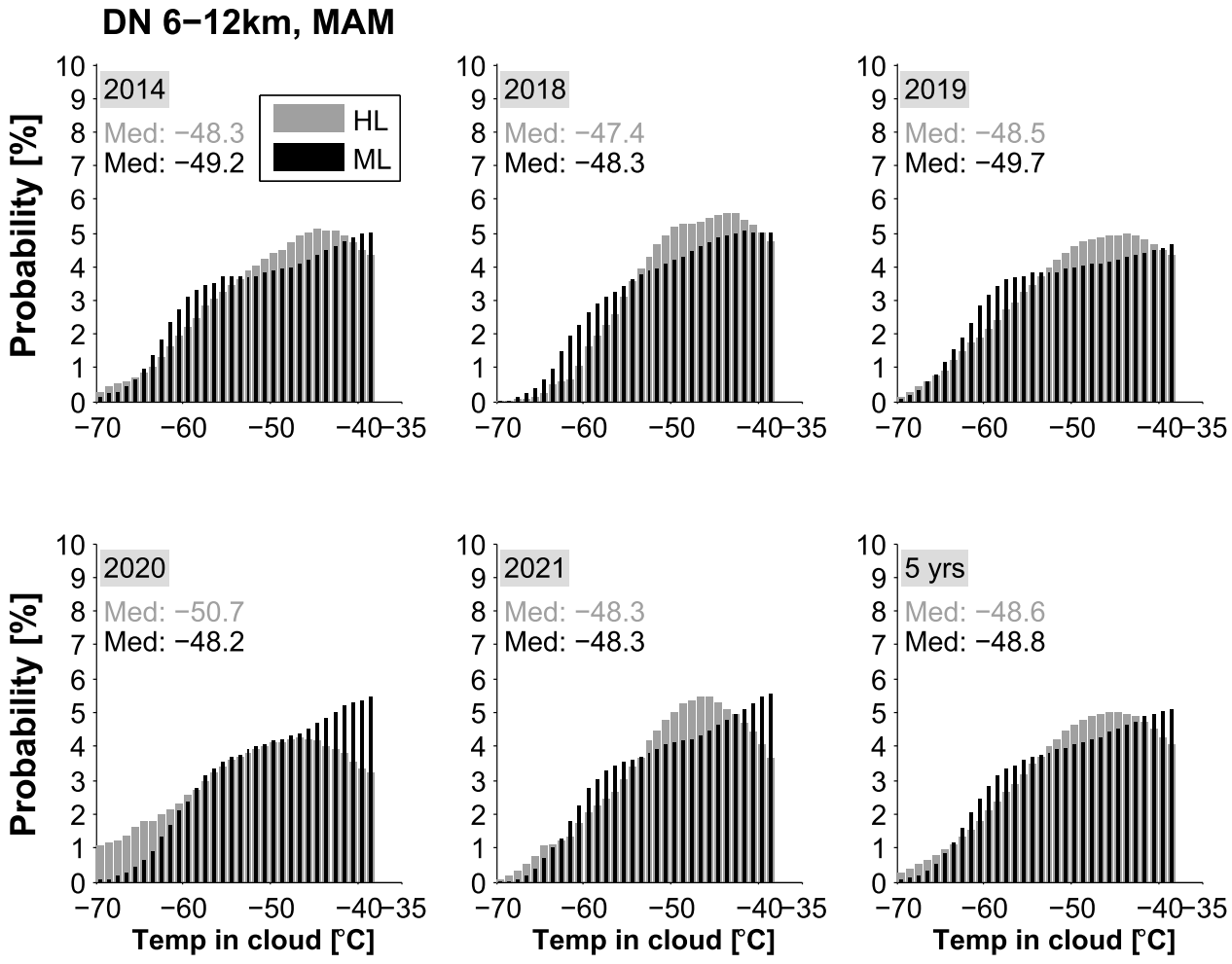

Figure 8. Comparison of temperatures inside cirrus clouds within different latitudes in spring. The histograms at HL are shown in gray and at ML in black with the medians indicated in the inset. In general, their distributions show a consistence in different years at different latitudes, respectively. The formation of cirrus clouds at ML took place with the maximum occurrence at temperatures of -38°C, with a "shoulder" for temperatures down to -60°C, and a long tail extending to lower temperatures. Cirrus clouds at HL, however, occurred with the maximum probability at ∼-45°C and also with a long tail extending to lower temperatures.